Transient Responses of a Coupled Ocean–Atmosphere Model to Gradual Changes of Atmospheric CO_2. Part II: Seasonal Response

S. MANABE, M. J. SPELMAN, AND R. J. STOUFFER

Geophysical Fluid Dynamics Laboratory/NOAA, Princeton University, Princeton, New Jersey

(Manuscript received 26 April 1991, in final form 22 August 1991)

ABSTRACT

This study investigates the seasonal variation of the transient response of a coupled ocean–atmosphere model to a gradual increase (or decrease) of atmospheric carbon dioxide. The model is a general circulation model of the coupled atmosphere–ocean–land surface system with a global computational domain, smoothed geography, and seasonal variation of insolation.

It was found that the increase of surface air temperature in response to a gradual increase of atmospheric carbon dioxide is at a maximum over the Arctic Ocean and its surroundings in the late fall and winter. On the other hand, the Arctic warming is at a minimum in summer. In sharp contrast to the situation in the Arctic Ocean, the increase of surface air temperature and its seasonal variation in the circumpolar ocean of the Southern Hemisphere are very small because of the vertical mixing of heat over a deep water column.

In response to the gradual increase of atmospheric carbon dioxide, soil moisture is reduced during the June–July–August period over most of the continents in the Northern Hemisphere with the notable exception of the Indian subcontinent, where it increases. The summer reduction of soil moisture in the Northern Hemisphere is relatively large over the region stretching from the northern United States to western Canada, eastern China, southern Europe, Scandinavia, and most of the Russian Republic. During the December–January–February period, soil moisture increases in middle and high latitudes of the Northern Hemisphere. The increase is relatively large over the western portion of the Russian Republic and the central portion of Canada. On the other hand, it is reduced in the subtropics, particularly over Southeast Asia and Mexico.

Because of the reduction (or delay) in the warming of the oceanic surface due to the thermal inertia of the oceans, the increase of the moisture supply from the oceans to continents is reduced, thereby contributing to the reduction of both soil moisture and runoff over the continents in middle and high latitudes of the Northern Hemisphere. This mechanism enhances the summer reduction of soil moisture and lessens its increase during winter in these latitudes.

The changes in surface air temperature and soil moisture in response to the gradual reduction of atmospheric CO_2 are opposite in sign but have seasonal and geographical distributions that are broadly similar to the response to the gradual CO_2 increase described above.

1. Introduction

In Part I of this study (Manabe et al. 1991), the annually averaged response of a coupled ocean–atmosphere model to a gradual increase of atmospheric carbon dioxide is described, followed by a discussion of the processes that control the response. In Part II, the analysis is extended to the seasonal variation of the response.

Many studies have been made on the seasonal dependence of the equilibrium response of a climate model to an increase of atmospheric carbon dioxide (Manabe and Stouffer 1979, 1980; Held 1982; Washington and Meehl 1984; Hansen et al. 1984; Wilson and Mitchell 1987). They have shown that, over the Arctic and the surrounding regions and the coastal region of the Antarctic continents, the increase of surface air temperature is particularly large in winter, but small in summer (e.g., Manabe and Stouffer 1979; Schlesinger and Mitchell 1987). Some of these studies also indicate that soil moisture is reduced in summer over extensive, midcontinental regions of the North American and Eurasian continents. The present study will determine whether the change of climate obtained from the equilibrium response studies (Manabe et al. 1981; Mitchell et al. 1990) also occurs in a transient response experiment.

One should note that the models used for these equilibrium response studies are constructed by combining a general circulation model of the atmosphere with a vertically isothermal slab of water with a thickness of 50 m. In some of these models (e.g., Hansen et al. 1984), a heat flux at the bottom of the mixed-layer ocean is prescribed such that the geographical and seasonal variations of sea surface temperature and sea ice are realistic. An identical distribution of heat flux is also specified for the case of above-normal CO_2 concentration. This is in contrast to the transient re-

Corresponding author address: Dr. S. Manabe, Princeton University, Geophysical Fluid Dynamics Laboratory/NOAA, Forrestal Campus, US Route 1, P.O. Box 308, Princeton, NJ 08542.

sponse of a coupled ocean–atmosphere model in which the heat exchange between the mixed layer and deeper ocean layers changes with time. By comparing these two types of responses, we will evaluate how the temporal variation in the oceanic uptake of heat affects the CO_2-induced change of climate.

As noted in Part I, the vertical mixing of heat between the upper layer and deeper layers of the ocean is particularly pronounced in the circumpolar ocean of the Southern Hemisphere and in the northern North Atlantic. It will be shown that, over these oceans and their neighborhood, such intense vertical mixing can substantially alter not only the geographical pattern of climate change but also its seasonal variation.

2. Numerical experiments

In Part I, the basic strategy of the numerical experiments and the structure of the models used were discussed in detail. Therefore, only very brief accounts of these topics are included in this section.

a. Transient experiments

The coupled ocean–atmosphere model used for this experiment consists of a general circulation model of the World Ocean coupled to a general circulation model of the atmosphere. Heat and water budgets of the continental surface are included. The model has a global geography and seasonally varying insolation.

To study the response of the coupled ocean–atmosphere model to a gradual increase (or reduction) of atmospheric carbon dioxide, three 100-year integrations of the model were performed. Starting from an initial condition in a quasi-equilibrium state, the standard time integration of the coupled ocean–atmosphere model (hereafter referred to as the S integration) was performed with a normal concentration of atmospheric carbon dioxide. In addition, two 100-year integrations were performed from this identical initial condition. In one integration, the CO_2 concentration in the atmosphere is increased by 1% yr^{-1} (compounded), whereas it is reduced by the identical rate in the other integration. The rate of 1% yr^{-1} in the former integration is chosen because the radiative forcing of all greenhouse gases other than water vapor is currently increasing approximately at this rate (see, for example, Hansen et al. 1988 on the current trace gas trends). These two integrations with growing and decreasing CO_2 concentration are identified as the G and D integrations, respectively. The influences of a gradual increase and reduction of atmospheric carbon dioxide are evaluated by computing the differences between the G and S integrations and the D and S integrations, respectively. For convenience, the set of G and S integrations will be called the CO_2 growth experiment, while the D and S integrations will be called the CO_2 reduction experiment. (Note that the S integration is used for both experiments.)

To prevent the drift of the model away from the observed climate, the fluxes of both heat and water at the ocean–atmosphere interface are adjusted by amounts that vary seasonally and geographically. These adjustments do not change from one year to the next and are independent of the temporal variation of surface conditions. Nevertheless, temperature and salinity at the oceanic surface remain near the observed values in the standard (S) integration. The volume of sea ice, however, increases very slowly (0.3% yr^{-1}) in both the Arctic and circumantarctic oceans during the integration. Adjustments identical (in magnitude and distribution) to those used in the S integration are also performed in the G and D integrations.

Since the infrared absorptivity (or emissivity) of carbon dioxide is approximately proportional to the logarithm of its amount, the exponentially growing and decreasing concentrations of carbon dioxide generate thermal forcings similar in magnitude but having opposite sign. Thus, it is of interest to see whether the responses of the coupled model are also opposite in sign but similar in magnitude, indicating a linear relationship between the thermal forcing and the response of the model. Refer to Table 1 for a quick identification of the various integrations involved in the transient experiments.

b. Equilibrium experiments

One of the main goals of the present study is to investigate how the oceans affect the response of climate to a change of atmospheric carbon dioxide. For this

TABLE 1. Numerical experiments performed in this study.

	Experiments		Integrations	CO_2 concentrations
Transient response	CO_2 growth experiment	→	G	+1% yr^{-1}
			S	Normal
	CO_2 reduction experiment	→	D	−1% yr^{-1}
Equilibrium response	CO_2 doubling experiment	→	E2X	2·(Normal)
			ES	(Normal)
	CO_2 halving experiment	→	EX/2	(Normal)/2

purpose, one can compare the transient response of the coupled ocean–atmosphere model to the equilibrium response of the same model. Such a comparison has been made in several studies conducted at the Geophysical Fluid Dynamics Laboratory of NOAA (Bryan et al. 1982; Spelman and Manabe 1984; Bryan et al. 1988; Manabe et al. 1990).

As explained in the Introduction, the model used for the equilibrium experiment in the present study differs from the coupled ocean–atmosphere model used for the transient experiment. Although its atmospheric and land-surface components are identical to those of the coupled ocean–atmosphere model, its oceanic component is a simple mixed-layer ocean model, which is a 50-m–thick slab of vertically well-mixed water. The oceanic component contains a highly idealized scheme for sea ice prediction, which is similar to the scheme in the coupled ocean–atmosphere model, though the drift of sea ice by ocean currents is not incorporated. The rate of heat exchange between the mixed layer and the deeper layer of the oceans is prescribed such that the seasonal and geographical distributions of observed sea surface temperature and sea ice thickness are maintained. This model will hereafter be identified as the atmosphere–mixed-layer ocean model, or more simply as the AM model.

In addition to the standard integration with the normal concentration of atmospheric carbon dioxide, two additional integrations were performed over the period of 40 years assuming twice and half the normal CO_2 concentration. The heat flux, which is prescribed at the bottom of the mixed layer in these two integrations, is identical to the flux prescribed in the standard integration. Toward the end of each integration the climate of the AM model is close to the state of equilibrium and exhibits very little trend. The quasi-equilibrium climates were computed for the cases of twice and half the normal CO_2 concentrations by computing the average states of the model over the last 10 annual cycles of the two integrations. For the convenience of identification, these two quasi equilibria are called E2X and EX/2, respectively. The quasi-equilibrium climate, which was obtained from the last 10 annual cycles of the standard integration and was described in the preceding paragraph, will be identified as ES. By subtracting the ES from the E2X and the ES from the EX/2, the equilibrium responses to the doubling and halving of atmospheric carbon dioxide were evaluated.

The equilibrium response of the AM model to the doubling (or halving) of atmospheric carbon dioxide can be compared with the transient response of the coupled ocean–atmosphere model at the time of CO_2 doubling (or halving). It represents the maximum response without the reduction (or delay) due to the thermal inertia of the ocean. The difference between the two responses indicates how the oceans help in delaying the response of climate to increasing (or decreasing) concentration of atmospheric carbon dioxide. Although the oceanic uptake of heat changes throughout the time-dependent response of the coupled ocean–atmosphere model, the heat flux at the bottom of the mixed-layer ocean does not change in the equilibrium response of the AM model. Thus, the comparison between the transient and equilibrium responses should reveal how the temporal variation in the oceanic uptake of heat alters the transient response of climate. Refer to Table 1 for a quick identification of the integrations involved in the equilibrium experiments.

In the transient experiments, the atmospheric concentration of CO_2 doubles (or halves) about 70 years after the beginning of the experiment. For comparison with the equilibrium experiment, the transient response at the time of the CO_2 doubling (or halving) is obtained by computing the difference between the G (or D) integration averaged over the 60th–80th-year period and the S integration averaged over the entire 100-year period. This is done unless otherwise noted.

3. Simulation of seasonal variation

The performance of the present model in simulating the annual mean state of the coupled ocean–atmosphere system was reviewed in Part I of this study. In this section, the seasonal variation of the climate as simulated by the coupled model in the standard (S) integration will be described briefly.

a. Temperature

The simulated and observed difference in monthly averaged surface air temperature between August and February is shown in Fig. 1. The model approximately reproduces the regions of local maximum in the annual range of surface air temperature over northwestern Siberia and northern Canada in the Northern Hemisphere and the southern ends of South America and Africa in the Southern Hemisphere. Because of a strong maritime influence, the annual range of the coupled model is relatively small over Europe, in agreement with observations. In general, the annual range of surface air temperature over continents is at a maximum around 65° latitude in the Northern Hemisphere, influenced by the snow albedo feedback process. In the Southern Hemisphere where the size of the continents is small, the annual range of surface air temperature over continents is usually smaller than the Northern Hemisphere. Although the range is at a maximum over the Antarctic continent, it is much smaller than the maximums over the continents of the Northern Hemisphere because the positive feedback effect of snow is small over an ice sheet with high surface albedo.

b. Precipitation

Figures 2 and 3 compare the distributions of simulated precipitation during the periods of December–

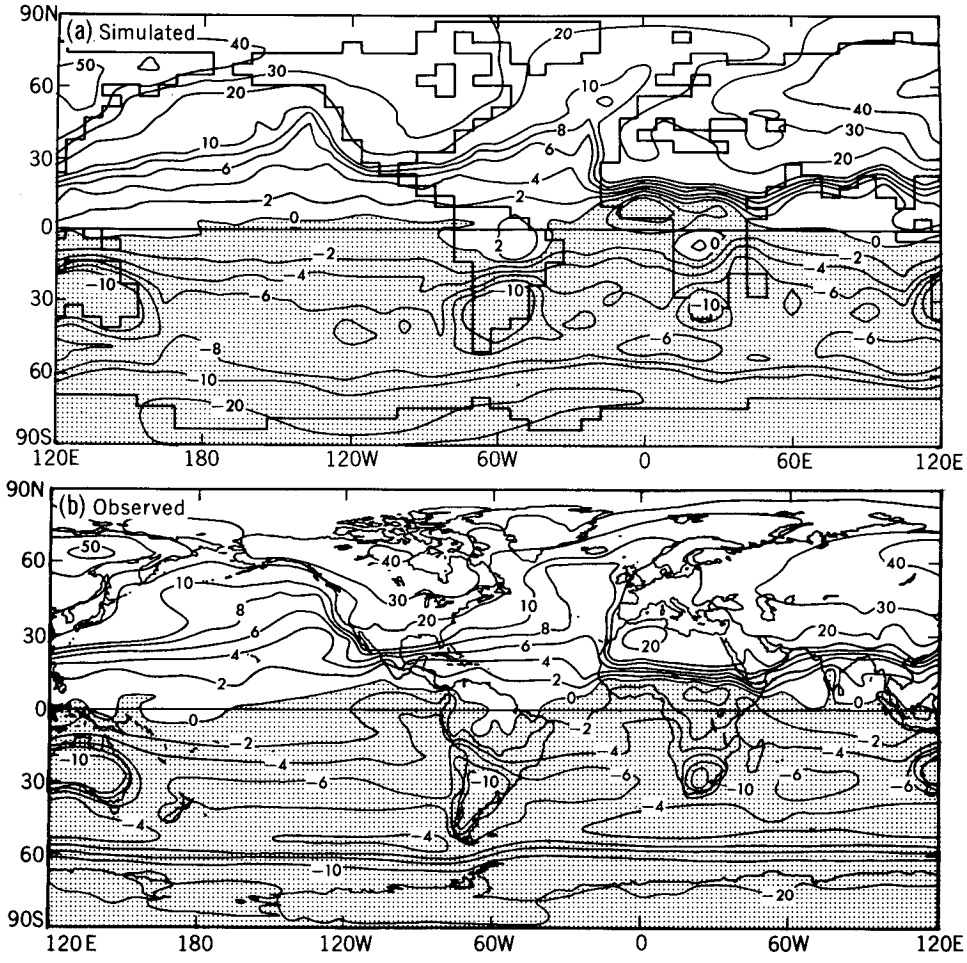

FIG. 1. The geographical distribution of the difference in monthly mean surface air temperature (°C) between August and February. (a) Simulated by the S integration of the coupled model averaged over the 60th–80th-year period. (b) Observed (Crutcher and Meserve 1970; Taljaard et al. 1969). The contour interval of 2°C changes to 10°C when the absolute value of the temperature difference is greater than 10°C.

February and June–August with those observed. In general, the model overestimates the precipitation in high latitudes of both hemispheres. This results from the bias of the present low-resolution spectral model toward overestimating the poleward transport of moisture. In both the December–February and June–August periods, the rate of simulated precipitation is too small in the tropical rainbelt of the summer hemisphere and is too large in the subtropical dry belt of the winter hemisphere. Because of the bias of the low-resolution model toward underestimating the subtropical highs and the intensity of the Hadley cell that straddles the equator, the precipitation is too small in the rising branch of the cell and too large in its sinking branch. Despite the shortcomings of simulation identified above, the model mimics the shifts of the tropical rainbelt and the middle latitude rainbelts of the Northern Hemisphere between the December–February and June–August periods.

4. Thermal response

a. Zonal mean response

Figure 4 compares the transient response of zonally averaged surface air temperature at the time of CO_2 doubling with its equilibrium response to CO_2 doubling. In high latitudes of the Northern Hemisphere, the increase of zonal-mean surface air temperature in the transient experiment is relatively large in winter and is at a maximum around November, but is at a minimum in summer in qualitative agreement with the equilibrium experiment. In the Southern Hemisphere, the winter maximum is missing in the transient response of surface air temperature over the Antarctic continent and its immediate vicinity, in sharp contrast to its equilibrium response, which has the pronounced seasonal variation.

The transient and equilibrium responses of zonal-

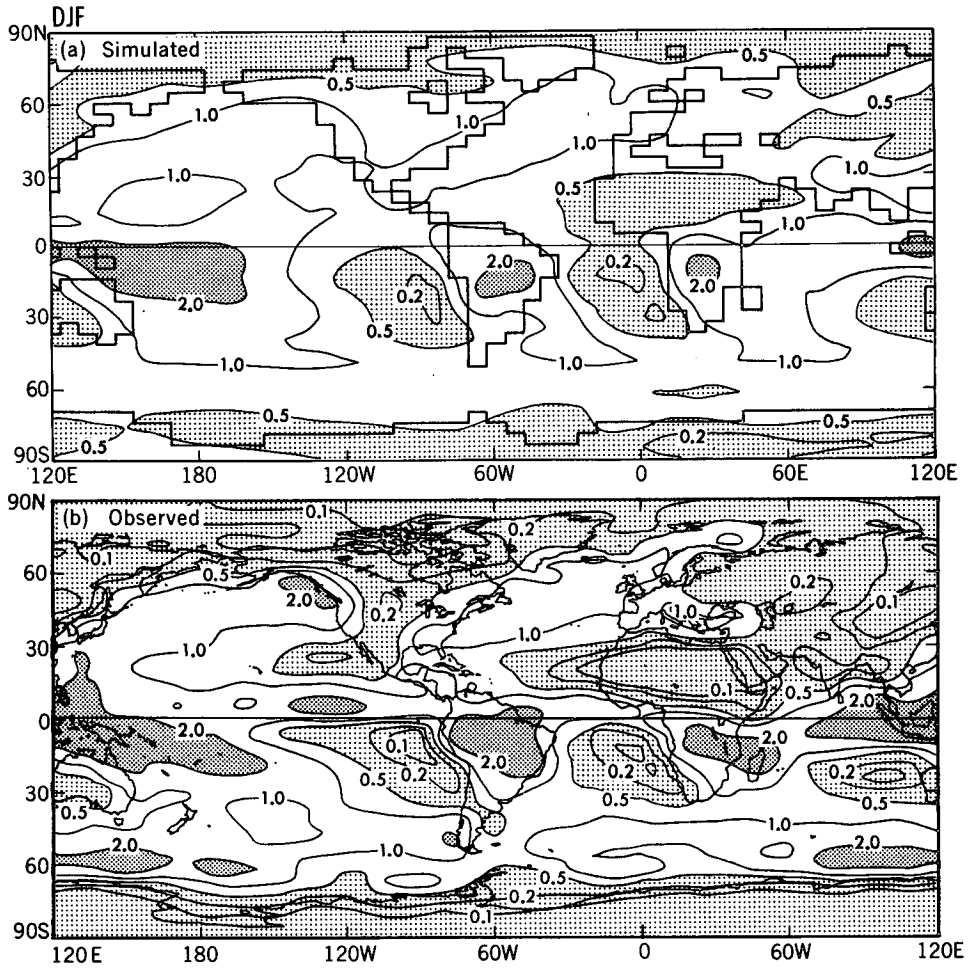

FIG. 2. The geographical distribution of the rate of precipitation (m yr^{-1}) averaged over the December–February period. (a) Simulated by the S integration of the coupled model averaged over the 60th–80th-year period. (b) Observed (Jaeger 1976).

mean surface air temperature to the halving of atmospheric CO_2 are shown in Fig. 5. The latitudinal and seasonal dependence of these responses is qualitatively similar to the corresponding responses to the doubling of atmospheric CO_2. The signs of temperature changes, however, are opposite between the two sets of responses.

The results described above indicate that, in high latitudes of the Northern Hemisphere, the seasonal variation of the changes in zonal-mean surface air temperature in the transient experiments is qualitatively similar to the equilibrium experiments. To identify the physical mechanisms responsible for these changes, we analyzed the surface heat budget of the Arctic Ocean for the transient CO_2 growth and CO_2 doubling equilibrium experiments. We found that the changes in the surface heat budget of the Arctic Ocean in these two experiments are qualitatively similar to each other. They are also very similar to the results of the equilibrium experiment conducted earlier by Manabe and Stouffer (1979, 1980) and Held (1982). Refer to their papers for a detailed illustration of the seasonal variation of the changes in various heat-balance components over the Arctic Ocean.

The analysis of the CO_2 growth experiment indicates that, in summer, the absorption of heat by the Arctic Ocean increases significantly in response to the gradual increase of atmospheric carbon dioxide. Despite the temperature increase in the lower model troposphere, the surface temperature of the Arctic Ocean fails to increase because it is anchored at the freezing point due to the melting of sea ice. Accordingly, the inversion of the vertical temperature gradient intensifies in the near-surface layer of the atmosphere, thereby increasing the downward flux of sensible heat and reducing the net upward flux of longwave radiation. Both of these flux changes constitute net heat gain for the oceanic surface. In addition, the reduction of sea ice is accompanied by the reduction of surface albedo, and accordingly, the increased surface absorption of solar energy

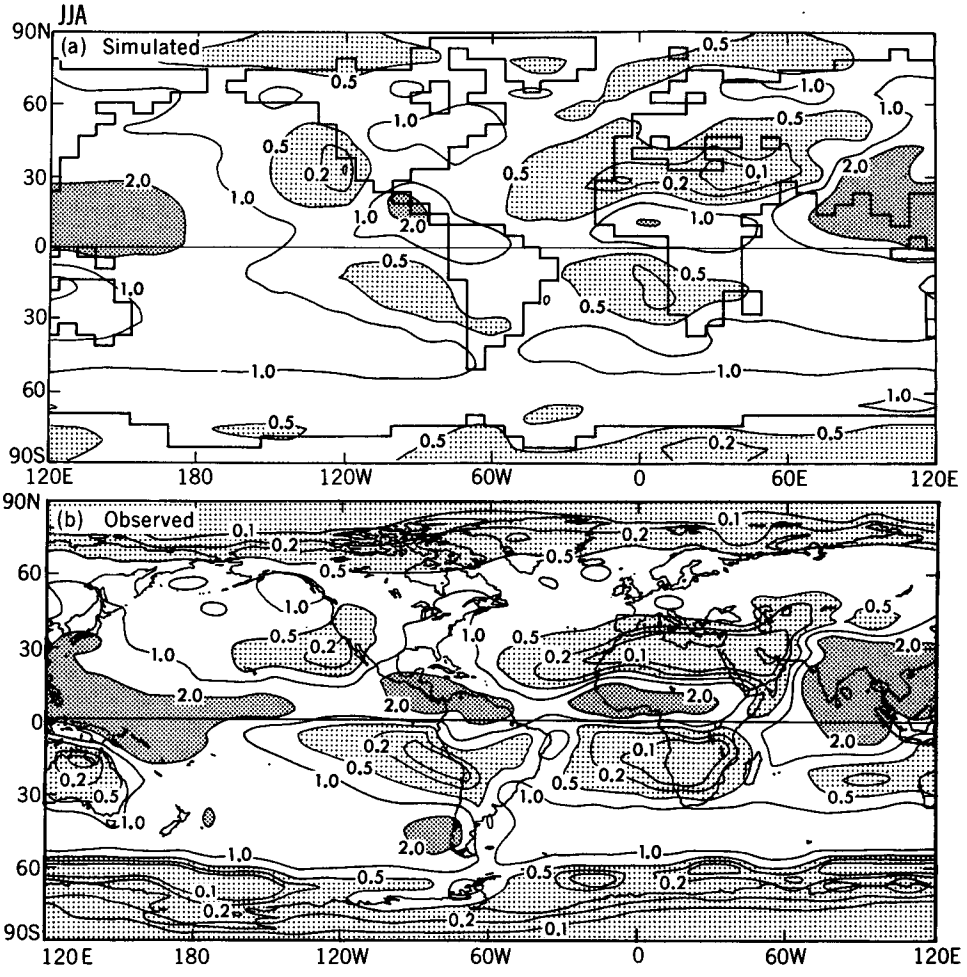

FIG. 3. Same as Fig. 2 averaged over the June–August period.

over the Arctic Ocean. These gains in the surface heat budget contribute to the increase of heat storage in the Arctic mixed layer in summer. The increased heat storage, in turn, slows down the growth of sea ice from fall to winter.

The enhanced summer infusion of heat into the mixed-layer ocean is compensated by the increase of the conductive heat loss through thinner sea ice during the cold season. Thus, the annual heat balance of the mixed-layer ocean is maintained. The heat exchange between the mixed layer and the deep Arctic Ocean is small and hardly changes because of the existence of a halocline with very stable stratification. The increase of upward conductive heat flux due to the reduction of sea ice, in turn, results in the increase of the upward sensible heat flux into the lower model atmosphere, markedly enhancing the increase of the surface air temperature in the late fall and early winter as shown in Figs. 4a and 4b.

The seasonal variation of the change of zonal-mean sea surface temperature in the transient CO_2 growth experiment is illustrated in Fig. 6. In high latitudes of the Northern Hemisphere, the sea surface warming increases rapidly from May to September due to the enhanced summer absorption of heat by the mixed-layer ocean. The warming is reduced from November to March due to the larger upward heat conduction through thinner sea ice.

In sharp contrast to the situation at the Arctic Ocean, the seasonal variation of the surface heat budget of the circumpolar ocean of the Southern Hemisphere obtained from the transient experiments is completely different from the corresponding budget in the equilibrium experiments. In the transient CO_2 growth experiment, for example, the temperatures of the mixed-layer ocean and overlying air hardly change in the circumpolar ocean because of the convective heat exchange between the mixed layer and deeper ocean with large thermal inertia. On the other hand, the changes of both surface air temperature and sea ice thickness in the equilibrium experiment are large and vary with season. In short, the seasonal variation of the change

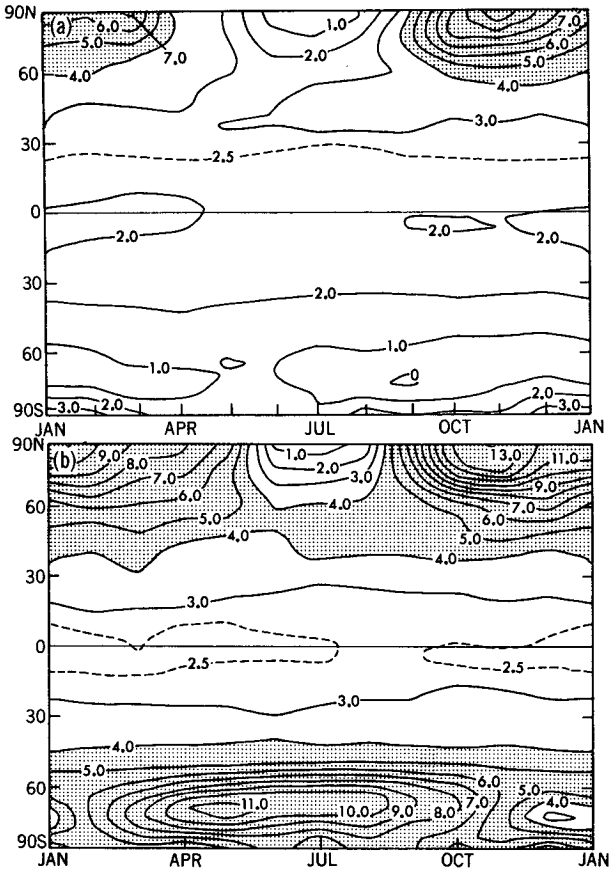

FIG. 4. Seasonal and latitudinal variation of the difference in zonal-mean surface air temperature (°C) between (a) the G and S integrations, and (b) the E2X and ES integrations. The results from the G and S integrations represent averages over the 60th–80th-year period. Shading covers the areas where the difference exceed 4°C.

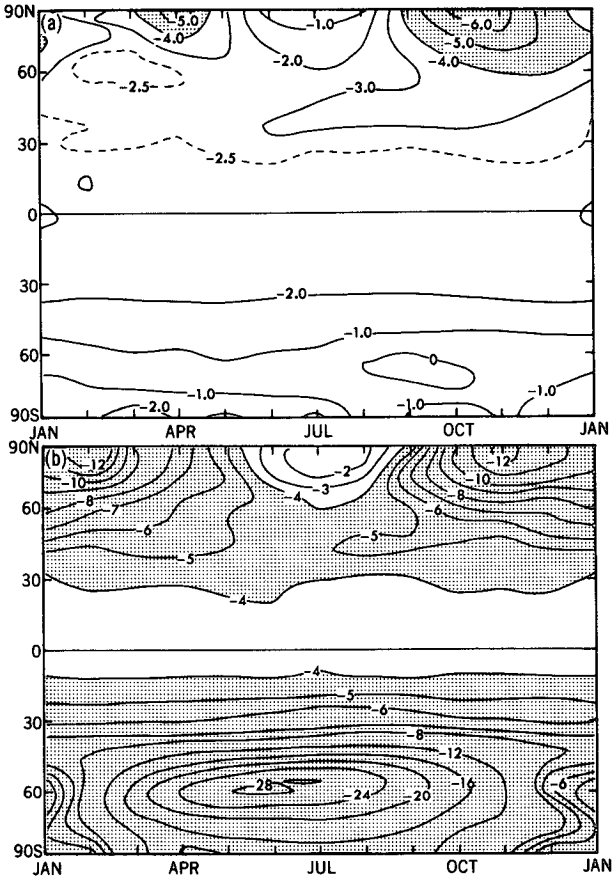

FIG. 5. Seasonal and latitudinal variation of the difference in zonal-mean surface air temperature (°C) between (a) the D and S integrations, and (b) EX/2 and ES integrations. The results from the D and S integrations represent averages over the 60th–80th-year period. Shading covers the areas where the difference is less than −4°C. In (b), the contour interval changes to 4°C below values of −8°C in the Southern Hemisphere.

of surface air temperature in the circumpolar ocean of the Southern Hemisphere is quite different between the transient and equilibrium response experiments because the changes of sea surface temperature and sea ice thickness and their seasonal variation in the former experiment are damped out, due to the heat exchange between the mixed layer and deeper layer of the oceans.

To explore the convective mixing in the circumpolar ocean of the Southern Hemisphere, the rate of temperature change due to convective adjustment in the S integration is area averaged poleward of 60°S latitude and is shown in Fig. 7a. According to this figure, the convective temperature change is positive and large in the mixed layer of the ocean but is negative in the underlying, deep layers of the model ocean, indicating the occurrence of very deep convective overturning of water. The figure also indicates that the convective overturning predominates during the winter half of the year (i.e., from April to October) and is most active

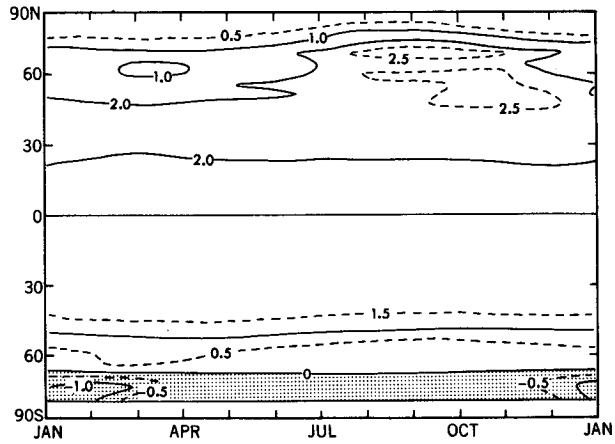

FIG. 6. The seasonal and latitudinal variation of zonal-mean sea surface temperature difference (°C) between the G (60th–80th year) and the S (0–100th year) integrations. Shading covers the regions where the difference is less than 0°C.

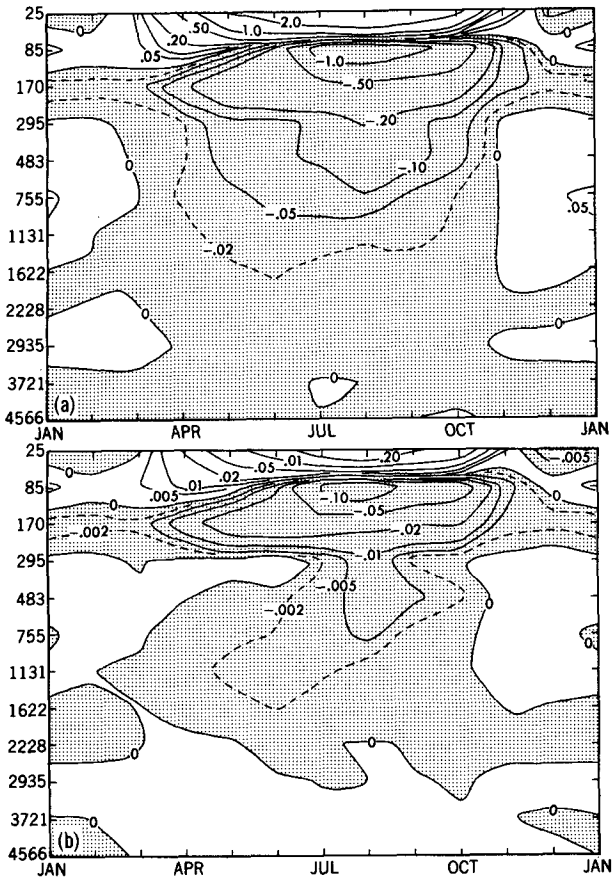

FIG. 7. The rates of (a) temperature change (°C yr^{-1}) and (b) salinity change (psu yr^{-1}) attributable to convective adjustment as a function of season and oceanic finite-difference level, area averaged poleward of 60°S latitude in the Southern Hemisphere. The rate is time averaged over the 60th–80th year of the S integration.

around August. A similar feature is evident in the zonal mean change of salinity (Fig. 7b) due to convective overturning, underscoring the strong influence of salinity upon the convective activity. As the season proceeds from fall to winter, the temperature of the mixed-layer ocean is reduced and its salinity increases due to the enhanced production of sea ice. Thus, the density of the water in the near-surface layer increases, promoting convective overturning of the water. It is notable that the layer of very small negative convective temperature change actually extends to the bottom of the model ocean in winter due to the very deep overturning of the water in the Ross and Weddell seas. The convective mixing in the circumpolar ocean also penetrates deeply in the G integration but is somewhat weaker than the S integration described above. As discussed in Part I of this study, the reduction of surface salinity resulting from the increase of freshwater supply at the oceanic surface is mainly responsible for the weaker convective activity in the G integration. As one might expect, the convective activity in the D integration is significantly more intense than the S integration.

In assessing the results from the analysis of vertical convective mixing in the ocean, it is important to note that the ocean model used here has other subgrid-scale mixing processes, such as isopycnal mixing (see appendix A of Manabe et al. 1991). In the circumpolar ocean of the Southern Hemisphere where the isopycnal surface has a very steep slope, isopycnal mixing often acts complementary to convective overturning and may provide some vertical mixing, even during the warm season. The combined effect of these subgrid-scale mixing processes and their seasonal variation will be the subject of future investigation.

Figure 8 indicates that, in February, the warming in high latitudes of the Northern Hemisphere is particularly large in the near-surface layer of the model troposphere and sharply decreases with increasing altitude. In August when the increase of surface air temperature over the Arctic Ocean is small as discussed above, the warming increases with increasing altitude. A similar feature is evident in both August and February over the circumpolar ocean of the Southern Hemisphere where the change of surface air temperature is small throughout the year. In the model ocean, the pattern of the warming is very similar between February and August below the depth of approximately 150 m, in-

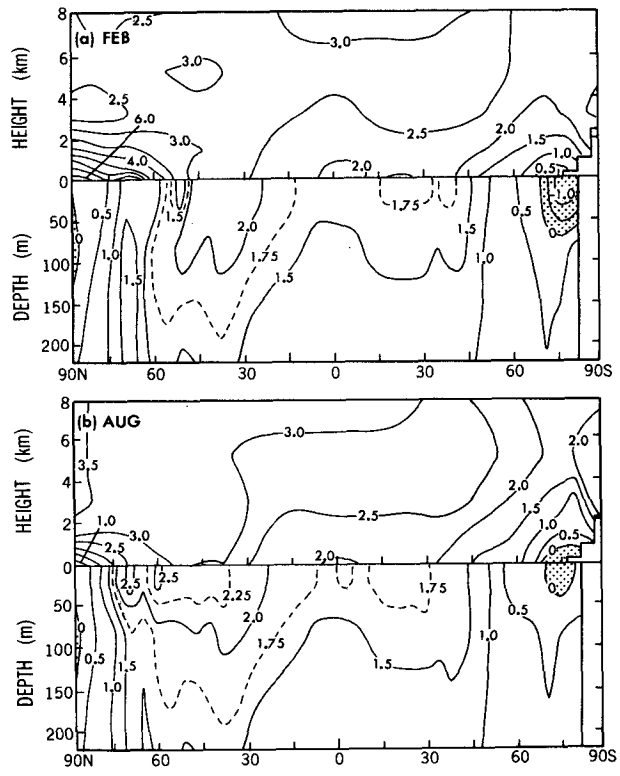

FIG. 8. The latitude–height (depth) distribution of the difference in zonally averaged, monthly mean temperature (°C) of the troposphere and upper ocean between the G and S integrations for (a) February and (b) August. The difference represents the 20-year average over the 60th–80th-year period of both integrations.

dicating that the seasonal variation of the zonal mean warming hardly penetrates below this depth. In the northern North Atlantic and the circumpolar ocean of the Southern Hemisphere with exceptionally deep convection, the seasonal variation of the temperature change is also too small to be detectable below the near-surface layer because the convective mixing of heat extends into the deep ocean with large thermal inertia as discussed above.

b. *Geographical response*

In the CO_2 growth experiment, the increase of Northern Hemisphere surface air temperature in winter is particularly large over the Arctic Ocean (Fig. 9a). Because of the positive feedback effect of snow cover, which extends to lower latitudes than sea ice in winter, the regions of a relatively large increase of surface air temperature extend down to 40°N latitude over both the Eurasian and North American continents. In sharp contrast to the situation in winter, the increase of surface air temperature over the Arctic Ocean in summer is relatively small (Fig. 9b) as discussed above. Thus, there is a marked reduction of the seasonal range of surface air temperature by several degrees celsius in high latitudes of the Northern Hemisphere (Fig. 9c). In middle latitudes, the warming is particularly pronounced over both the Eurasian and North American continents due to the reduction of soil moisture and evaporative ventilation in summer. In short, both snow albedo feedback in winter and enhanced midcontinental dryness in summer account for the larger increase of annual mean surface air temperature over continents as compared with oceans in middle latitudes (see Fig. 12 of Part I). It is also notable that the increase of surface air temperature is relatively small in the North Atlantic around 45°–60°N latitudes in both winter and summer. As discussed in Part I, the increase of annual mean sea surface temperature is also small in this region of the model Atlantic.

In the Southern Hemisphere, the seasonal variation of the change of zonal-mean surface air temperature is much smaller than in the Northern Hemisphere, as noted already. In both seasons, the change of surface air temperature is at a minimum in the circumpolar ocean and becomes larger with decreasing latitudes. The change is also larger near the South Pole.

The geographical distribution of sea ice thickness also changes substantially in response to the gradual increase of atmospheric carbon dioxide as indicated in Figs. 10 and 11. Over the Arctic Ocean, both coverage and thickness of sea ice are reduced markedly in summer (Figs. 10b and 10d). Though the coverage of Arctic sea ice is reduced only slightly in winter (Figs. 10a and 10c), its thickness is reduced substantially in response to the increase of atmospheric carbon dioxide. In sharp contrast to the situation over the Arctic Ocean, the change of sea ice is relatively small in the circumpolar ocean of the Southern Hemisphere, with the exception of the Weddell and Ross seas, where it increases substantially from the S to G integrations (Figs. 11a and 11c; Figs. 11b and 11d) despite the increase of atmospheric carbon dioxide. Because of the reduction of surface salinity due to the increased water supply at the oceanic surface, the convective mixing between the mixed layer and deeper ocean becomes less frequent, slightly lowering surface water temperature and increasing sea ice thickness in both the Weddell and Ross seas, as discussed in Part I of this study.

5. Hydrologic response

Part I of this study shows how the changes of atmospheric carbon dioxide affect the annually averaged, hydrologic behavior of the atmosphere. This section evaluates the seasonal variation of the hydrologic responses of the model to the gradual changes of atmospheric carbon dioxide.

As noted in the Introduction, the equilibrium responses of some climate models to increased atmospheric carbon dioxide include a reduction of soil moisture over extensive, midcontinental regions of the North American and Eurasian continents (Manabe et al. 1981; Mitchell et al. 1987; Manabe and Wetherald 1987). However, other models fail to produce a similar summer reduction of soil moisture (see, for example, Meehl and Washington 1988; Hansen et al. 1984; and the reviews by Kellog and Zhao 1988; Zhao and Kellog 1988; Schlesinger and Mitchell 1987). According to Meehl and Washington (1988) and Mitchell and Warrilow (1987), the reduction of soil moisture in summer critically depends upon spring soil wetness in the control experiment. When soil is unrealistically dry in the control simulation, evaporation from soil fails to increase significantly in the doubled CO_2 experiment despite the increase of radiative energy available for evaporation, thereby preventing the reduction of soil moisture. Recently, it was noted by Mitchell et al. (1990) that a summer reduction of soil moisture is simulated by three different climate models with higher computational resolution. It is of interest to examine whether or not a similar change of soil moisture occurs in the transient experiment conducted here.

a. *Zonal mean response*

Figure 12b indicates that, in the transient CO_2 growth experiment, zonal mean soil moisture is reduced in summer at most latitudes of the Northern Hemisphere, particularly around 45° and 60°N. On the other hand, zonal-mean soil moisture increases during winter in middle and high latitudes, though it is reduced around 25°N latitude. In the Southern Hemisphere, it is also reduced in winter (i.e., April–September) in the subtropics. Thus, zonal-mean soil moisture at the continental surface is reduced during

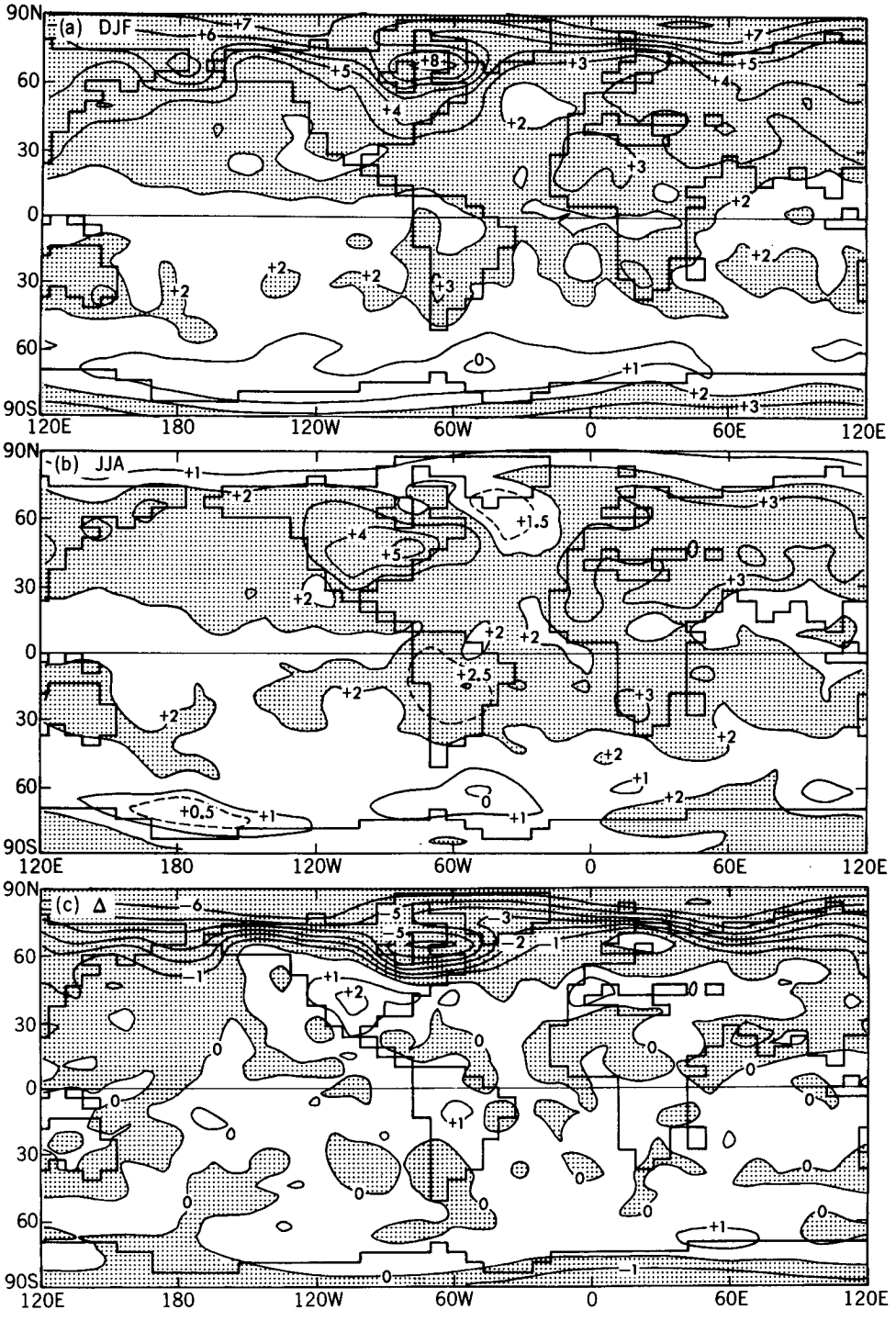

FIG. 9. The geographical distribution of the difference in surface air temperature (°C) between the G (60th–80th year) and S (0–100th year) integrations. (a) December–February. (b) June–August. Shading covers the regions where the difference is greater than 2°C. (c) The difference of (b) minus (a).

the May–September period over most latitudes between 65°N and 40°S.

The change of zonal-mean soil moisture in the CO_2 growth experiment is qualitatively similar to the soil moisture change from the equilibrium experiment, particularly in the Northern Hemisphere (Fig. 12c). As noted in Part I of this study, the distribution of the increase in surface air temperature from the transient

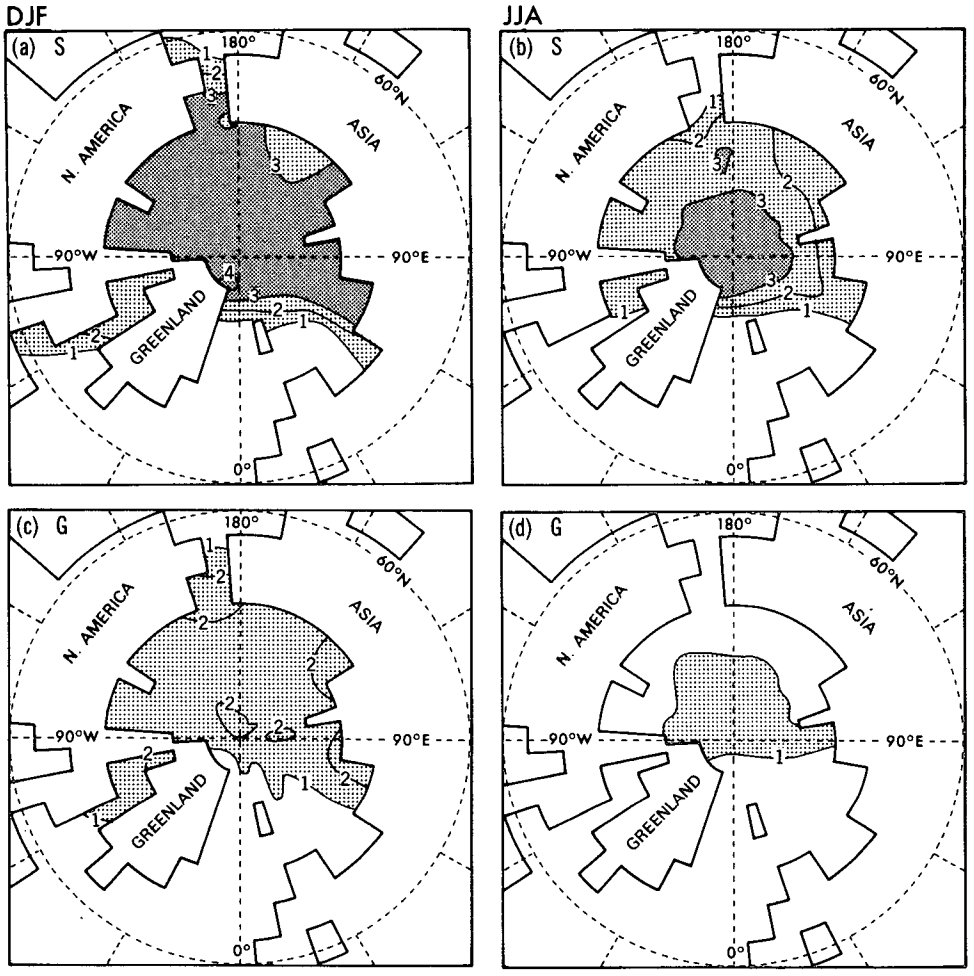

FIG. 10. The geographical distribution of seasonal mean sea-ice thickness over the Arctic Ocean. (a) The S (0–100th year) integration for December–February. (b) The S (0–100th year) integration for June–August. (c) The G (60th–80th year) integration for December–February. (d) The G (60th–80th year) integration for June–August. Light and dark shadings cover the regions where the thickness of sea ice exceeds 1 m and 3 m, respectively. Because of the very slow change of sea ice volume discussed in section 2, the distribution of sea ice thickness averaged over the 100-year period of the S integration is significantly thicker and less realistic than the initial distribution.

experiment is similar to the equilibrium experiment with the exception of the northern North Atlantic, western Europe, and the circumpolar ocean around the Antarctic Continent. Therefore, it is not surprising that the seasonal and latitudinal dependence of soil moisture change is qualitatively similar between the two experiments.

To assess the robustness of soil moisture changes described above, one can compare them with the results from the transient and equilibrium experiments in which atmospheric carbon dioxide is reduced (Fig. 13). The soil moisture changes from these two sets of experiments have opposite signs but qualitatively similar distributions. The antisymmetry of soil moisture between the two sets of experiments implies that the zonal mean changes of soil moisture described above are essentially CO_2-induced despite the possible contamination from the natural fluctuations of soil moisture.

To investigate the mechanisms responsible for the summer reduction of soil moisture in the CO_2 growth experiment, we analyzed the seasonal variations of various surface water balance components from both the S and G integrations over the 31°–53°N latitude belt where the summer reduction is relatively large (Fig. 14). It is expected that, with the increase of surface temperature, the evaporation from the oceans and most of the continental surface would increase. Figures 14b and 14c indicate that the rates of both rainfall and evaporation increase in middle latitudes with the exception of the summer season when soil moisture is small. Thus, one should evaluate the impact of precipitation change upon soil moisture by noting the concurrent change in evaporation.

An important factor affecting the imbalance between the gain by precipitation and the loss by evaporation is the timing of the rainy season in spring. The spring

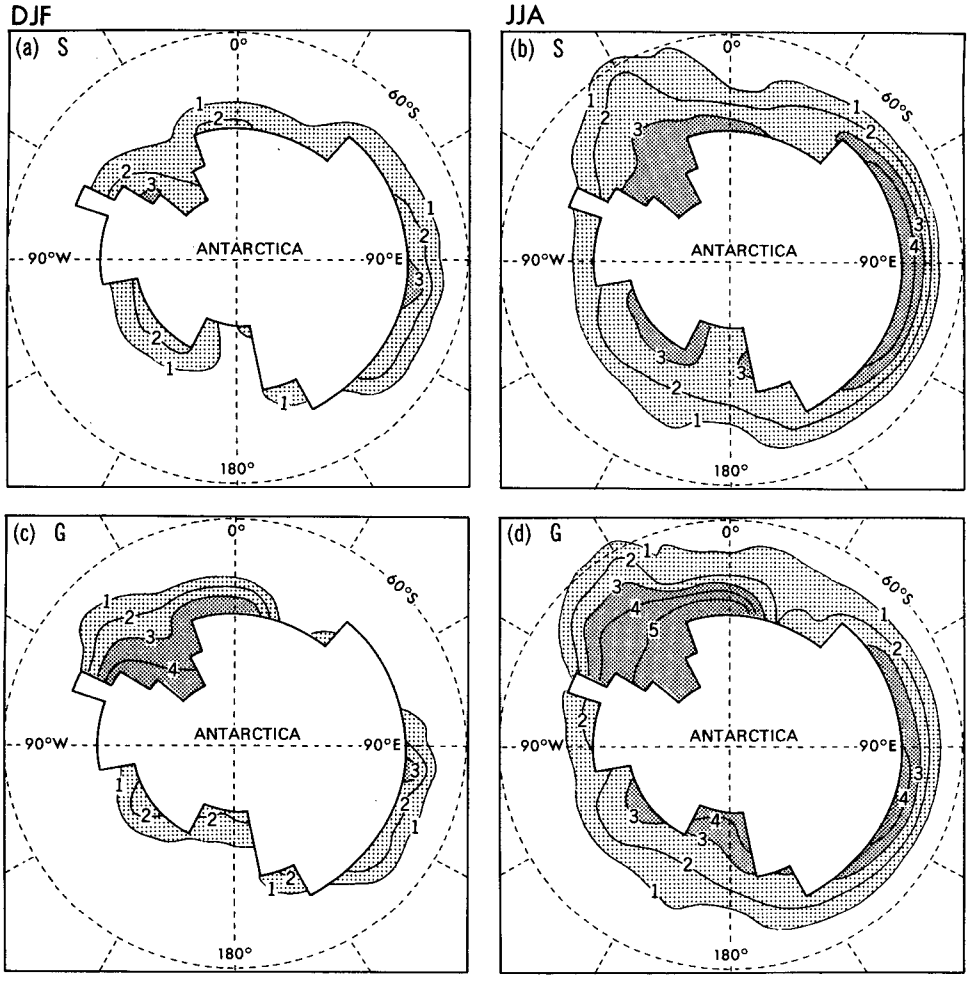

FIG. 11. The geographical distribution of seasonal mean sea-ice thickness over the circumpolar ocean of the Southern Hemisphere. (a) The S (0–100th year) integration for December–February. (b) The S (0–100th year) integration for June–August. (c) The G (60th–80th year) integration for December–February. (d) The G (60th–80th year) integration for June–August. Light and dark shadings cover the regions where the thickness of sea ice exceeds 1 m and 3 m, respectively.

period of relatively large rainfall ends earlier in the G than the S integration (Fig. 14b). Thus, the rapid reduction of soil moisture from spring to summer begins earlier, thereby making summer soil drier than it would be without the change in the timing of the rainy season. The change in the timing of the rainy season in spring is the consequence of the slight northward shift of the middle latitude rainbelt in the model (e.g., Manabe and Wetherald 1985, 1987). The shift of the rainbelt results from 1) the slight northward displacement of the axis of maximum zonal wind in the lower model troposphere, and 2) the penetration of warm, moisture-rich air into higher latitudes. Figure 15 indicates that precipitation in winter and spring increases to the north of the central axis of the middle latitude rainbelt (indicated by dashed lines), but is reduced to the south of the axis, implying the northward shift of the rainbelt. However, such a shift is not evident in summer when the rainbelt is poorly defined over major portions of continents and precipitation is reduced in the latitudinal range of relatively large rainfall, again contributing to the reduction of soil moisture in summer.

The change in snowmelt also contributes to the summer reduction of soil moisture around 45°N. Because of the warming, the spring period of rapid snowmelt ends earlier in the G than the S integration (Fig. 14b). Thus, the drying of soil from spring to summer begins earlier, again making the soil drier in summer. Furthermore, the earlier disappearance of snow cover increases the surface absorption of solar radiation and enhances the evaporation in late spring, thereby increasing the reduction of soil moisture in summer. The change of the snowmelt season is mainly responsible for the relatively large reduction of soil moisture in summer around 60°N latitude (Fig. 12b).

The summer reduction of soil moisture has a significant impact upon the heat budget of the continental surface. Because of the reduction of soil moisture, the

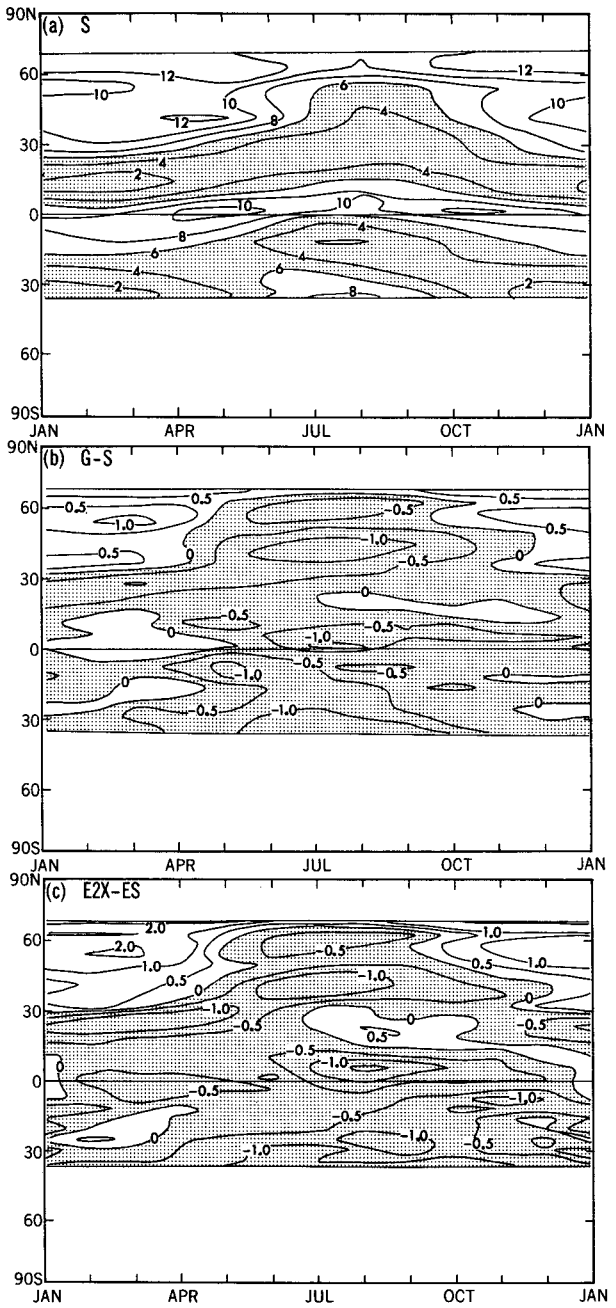

FIG. 12. The seasonal and latitudinal variation of zonal-mean soil moisture (cm) and its CO_2-induced changes. (a) Averages over the 60th–80th-year period of the S integration. (b) The difference between the G (60th–80th year) and S (60th–80th year) integrations. (c) The difference between the E2X and the ES integrations. In (a), the region of soil moisture less than 6 cm is shaded. In (b) and (c), the regions of negative soil moisture difference are shaded. The contour interval of 0.5 cm changes to 1.0 cm when the absolute value of the soil moisture difference is greater than 1 cm.

upward flux of sensible heat increases, whereas that of latent heat is reduced in summer. Thus, relative humidity, condensation of water vapor, and cloudiness are reduced in the lower model troposphere. The reduction of cloudiness, in turn, increases solar energy absorbed by the continental surface. The increase in evaporation resulting from the increased surface absorption of radiative energy, together with the reduction in precipitation rate due to the decrease of relative humidity mentioned above, further enhance the CO_2-induced reduction of soil moisture in summer.

Figure 12 indicates that, in both transient and equilibrium response experiments, the reduction of zonal-mean soil moisture in summer is relatively large around 45° and 60°N and is at a minimum around 50°N latitude. As discussed above, the belt of large soil moisture reduction around 45°N is partly attributable to the change in the middle latitude rainbelt, whereas the relatively large reduction around 60°N is mainly due to the earlier commencement of the spring to summer reduction of soil moisture resulting from the earlier termination of the snowmelt season.

In contrast to summer, the soil moisture in middle latitudes increases in winter when the rainbelt is located at the lowest latitudes (Fig. 15). The northward shift of the rainbelt results in the increase of precipitation

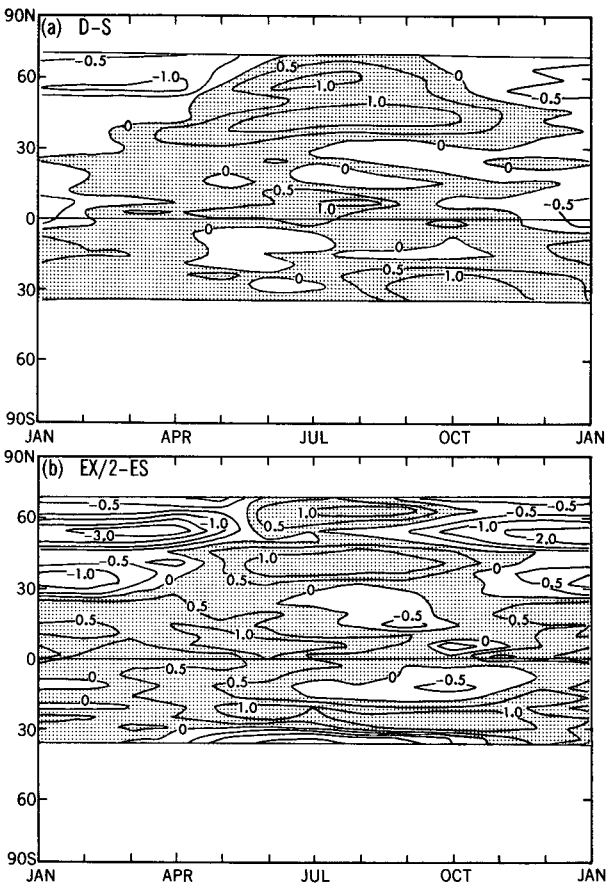

FIG. 13. The seasonal and latitudinal variation of the CO_2-induced changes in zonal-mean soil moisture (cm). (a) The difference between the D (60th–80th year) and S (60th–80th year) integrations. (b) The difference between the EX/2 and ES integrations. Shading indicates the regions of positive difference.

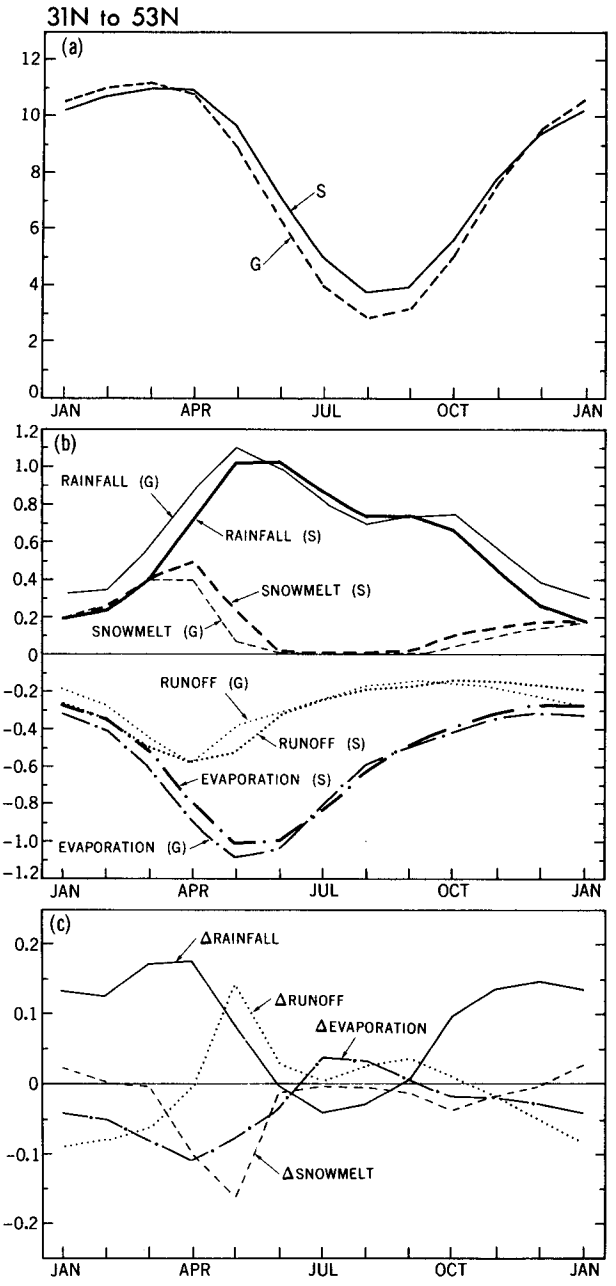

FIG. 14. The seasonal variation of soil moisture, surface water budget, and its CO_2-induced change averaged over the zonal belt ranging from 31° to 53°N. (a) Soil moisture (cm) from the S (solid line) and G (dashed line) integrations. (b) The surface water budget components (m yr^{-1}) from the S (thick lines) and G (thin lines) integrations. (c) The differences in surface water budget components (m yr^{-1}) between the G and S integrations. In (b) and (c), the sign convention is chosen such that a flux of water away from the surface has a negative sign representing water loss, whereas the flux toward the surface has a positive sign representing a water gain. The results from both the G and S integrations represent averages over the 60th–80th-year period.

in the northern half of the rainbelt; that is, middle latitudes (Fig. 14), contributing to the increase of soil moisture. The shift also results in the reduction of precipitation in the subtropics, located in the southern half of the rainbelt. Thus, soil moisture is reduced around 25°N in winter (Fig. 12b). A qualitatively similar but smaller reduction of soil moisture occurs in

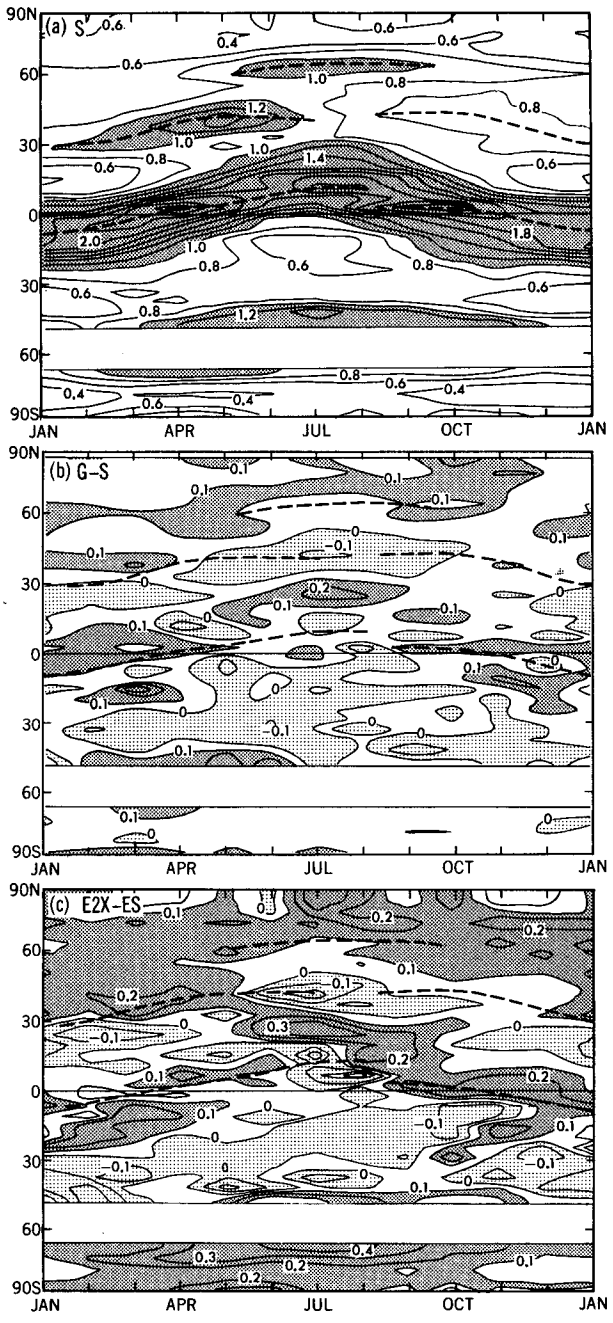

FIG. 15. The seasonal and latitudinal variation of precipitation rate (m yr^{-1}) and its CO_2-induced changes zonally averaged over continents. (a) Averages over the 60th–80th years of the S integration. (b) The difference in precipitation rate between the G (60th–80th year) and S (60th–80th year) integrations. (c) The difference in precipitation rate between the E2X and ES integrations. In (b) and (c), the thick dashed lines represent the central axis of the tropical and middle latitude rainbelts as indicated in (a).

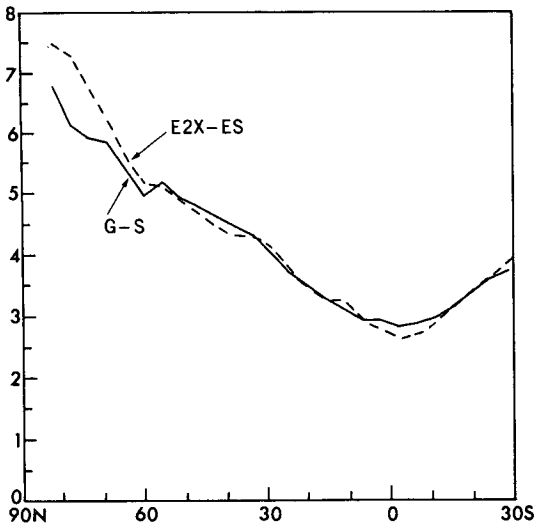

FIG. 16. The latitudinal profiles of the zonal mean difference in surface air temperature over continents between the G and S (solid line) and the E2X and ES (dashed line) integrations. The surface temperatures from the G and S integrations represent averages over the 80th–100th year and 0–100th year, respectively. Units are in °C.

the subtropics of the Southern Hemisphere during the June–August period (i.e., winter). In high latitudes, a marked increase of soil moisture in winter results mainly from the increase of snowmelt caused by the warming.

The mechanisms of the change of zonal-mean soil moisture described above are essentially similar to the corresponding change of soil moisture in the equilibrium response experiment conducted in the present and earlier studies (e.g., Manabe et al. 1981; Manabe and Wetherald 1985, 1987; Mitchell et al. 1987). However, there is an additional mechanism that reduces soil moisture and runoff in middle and high latitudes of the Northern Hemisphere throughout the year in the transient experiment.

In Part I of this study, it was shown that the land–sea contrast of the increase in surface air temperature of the Northern Hemisphere is more pronounced in the transient CO_2 growth experiment than in an equilibrium experiment with comparable overall warming. The enhanced land–sea contrast in the transient experiment is attributable to the reduction (or delay) in the surface warming of the oceans with large thermal inertia. The delay in the surface warming, in turn, delays the increase of evaporation from the oceanic surface, and accordingly, of precipitation over continents as well as oceans, contributing to the reduction of soil moisture and runoff (Rind et al. 1990). This can be demonstrated by comparing the hydrologic response of the continental surface from the equilibrium CO_2-doubling experiment with the corresponding response from the 80th–100th-year period of the CO_2 growth experiment at the stage of comparable warming. Over continents in the Northern Hemisphere and low latitudes of the Southern Hemisphere, the magnitudes of the zonal mean warming in these two responses are almost identical (Fig. 16) in contrast to the situation over the oceans. Thus, it is expected that the difference in the two hydrologic responses over Northern Hemisphere continents is mainly attributable to the difference in the moisture supply from the oceans. This is why the 80th–100th-year (rather than the 60th–80th-year) period of the CO_2 growth experiment is chosen for this particular analysis.

The ratio between the two responses of surface air temperature is close to one over continents (Fig. 17). However, the oceanic ratio is significantly smaller than the continental ratio in middle and high latitudes, un-

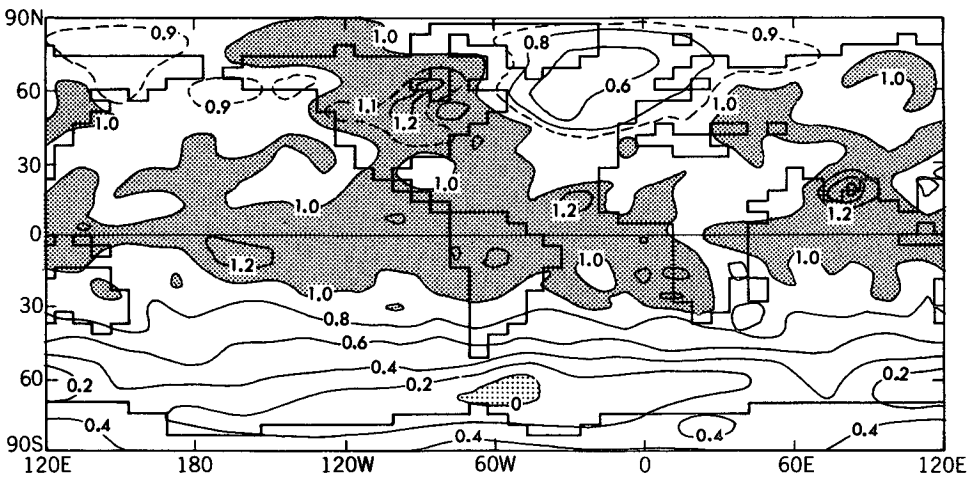

FIG. 17. The geographical distribution of the ratio of surface air temperature difference between the G and S integrations to the corresponding difference between the E2X and ES integrations. The surface air temperatures from the G and S integrations represent averages over the 80th–100th year and 0–100th year, respectively. Shading covers the region where the ratio is greater than 1.0.

derscoring the delay of the warming over the oceans in the transient experiment. In particular, the ratio over the Atlantic Ocean is relatively small, as discussed extensively in Part I of this study. In short, the land–sea difference in the warming is more pronounced in the transient experiment than the equilibrium experiment.

Figure 18 compares the latitudinal profile of the change in the zonal-mean soil moisture averaged over the 80th–100th-year period of the transient experiment with the corresponding profile from the equilibrium experiment. Northward of 30°N (i.e., in regions of oceanic delay in surface warming), the change of soil moisture is significantly different between the two experiments, although the magnitude of the warming over continents is practically identical between the two as noted above. For example, the soil moisture reduction during the June–August period is larger in the transient than the equilibrium experiment. During the December–February period, soil moisture in the former experiment does not increase as much as the latter. The impact of the delay in the warming of the oceanic surface is also evident in Fig. 19, which shows that the change in the precipitation minus evaporation is also reduced over continents at most latitudes northward of 30°N.

Table 2 indicates that, over the continents northward of 30°N latitude, the increase of area mean precipitation in the transient experiment (0.083 m yr^{-1}) is significantly less than the corresponding increase in the hand, the increases of area mean evaporation over the same continental regions are 0.041 and 0.043 m yr^{-1} in the former and the latter experiment, respectively, and are very similar to each other. Thus, the increase of the area mean runoff (computed here as the difference between precipitation and evaporation) over continents in middle and high latitudes of the Northern Hemisphere is significantly smaller in the transient experiment (0.042 m yr^{-1}) than in the equilibrium experiment (0.055 m yr^{-1}) despite the similarity in the magnitude of the continental warming between the two cases.

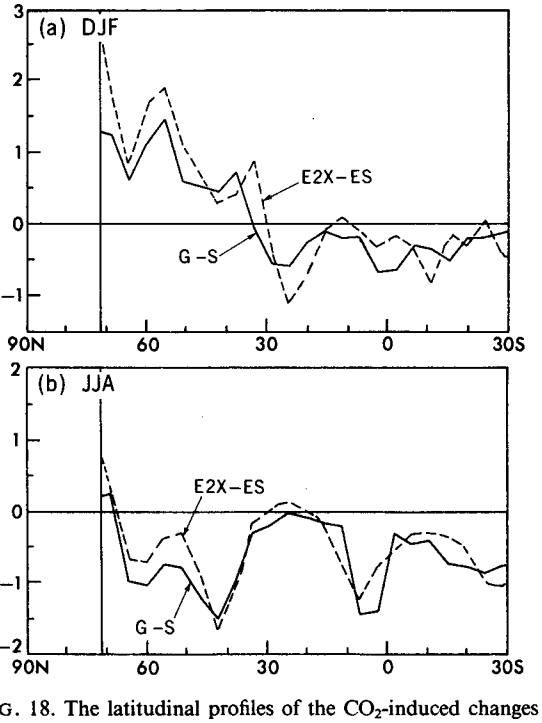

FIG. 18. The latitudinal profiles of the CO_2-induced changes in zonal-mean soil moisture (cm). (a) December–February. (b) June–August. Solid line represents the difference between the G (80th–100th year) and S (0–100th year) integrations. Dashed line represents the difference between the E2X and ES integrations.

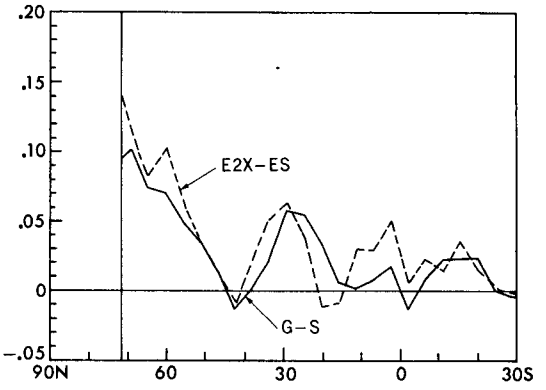

FIG. 19. The latitudinal profiles of the CO_2-induced changes in annually averaged, zonal mean difference between the rates of precipitation and evaporation (m yr^{-1}) over continents. Solid line represents the difference between the G (averaging period is 80th–100th year) and S (averaging period is 0–100th year) integrations. Dashed line represents the difference between the E2X and ES integrations.

Over the oceans northward of 30°N latitude, the area mean excess of precipitation over evaporation increases by 0.005 m yr^{-1} in the transient experiment, whereas it is reduced by 0.009 m yr^{-1} in the equilibrium experiment (see Table 2). This implies that, in middle and high latitudes of the Northern Hemisphere, the model atmosphere gains moisture from the oceanic surface in the transient response but loses it in the equilibrium response, supplying a larger amount of moisture to the continents in the former than the latter case. As explained already, this is due to the smaller oceanic warming in the transient experiment. In summary, the present analysis indicates that the delay in the warming of the oceanic surface contributes to the reduction of soil moisture and runoff in the transient experiment.

b. Geographical response

The geographical distribution of soil moisture change averaged over the 60th–80th-year interval of the CO_2 growth experiment is shown in Fig. 20. This figure indicates that, in the June–August period, soil moisture is reduced over most of the continental regions in both hemispheres. In middle latitudes of the Northern Hemisphere, the summer reduction of soil moisture is particularly large over the northern United States,

TABLE 2. Area mean rates of annual mean precipitation (p), evaporation (e), and $p - e$, averaged separately over continents and oceans from 30°N to 90°N latitude. The values from the G and S integrations represent averages over the 60th–80th year and the 0–100th year, respectively. Units are meters per year.

		Transient response			Equilibrium response		
		S	G	G − S	ES	E2X	E2X − ES
Continents	Precipitation	0.836	0.919	0.083	0.808	0.906	0.098
	Evaporation	0.519	0.560	0.041	0.501	0.544	0.043
	$p - e$	0.317	0.359	0.042	0.307	0.362	0.055
Oceans	Precipitation	0.882	0.943	0.061	0.912	1.004	0.092
	Evaporation	0.789	0.845	0.056	0.811	0.912	0.101
	$p - e$	0.093	0.098	0.005	0.101	0.092	−0.009

southern Europe, and extreme western and eastern portions of China, and is responsible for the relatively large reduction of zonal-mean soil moisture in summer around 45°N in Fig. 12b. The reduction is also large in the northwestern portion of Canada, Scandinavia, and most of the Russian Republic, with the exception of a region near the eastern end of Siberia, and accounts for the relatively large summer reduction of zonal-mean soil moisture around 60°N latitude in Fig. 12b. It is notable, however, that soil moisture increases over India in the June–August period, in qualitative agreement with the recent results from equilibrium studies conducted by use of models with relatively high computational resolution (Mitchell et al. 1990). In the Southern Hemisphere, the reduction of soil moisture during the June–August period (i.e., winter) is rela-

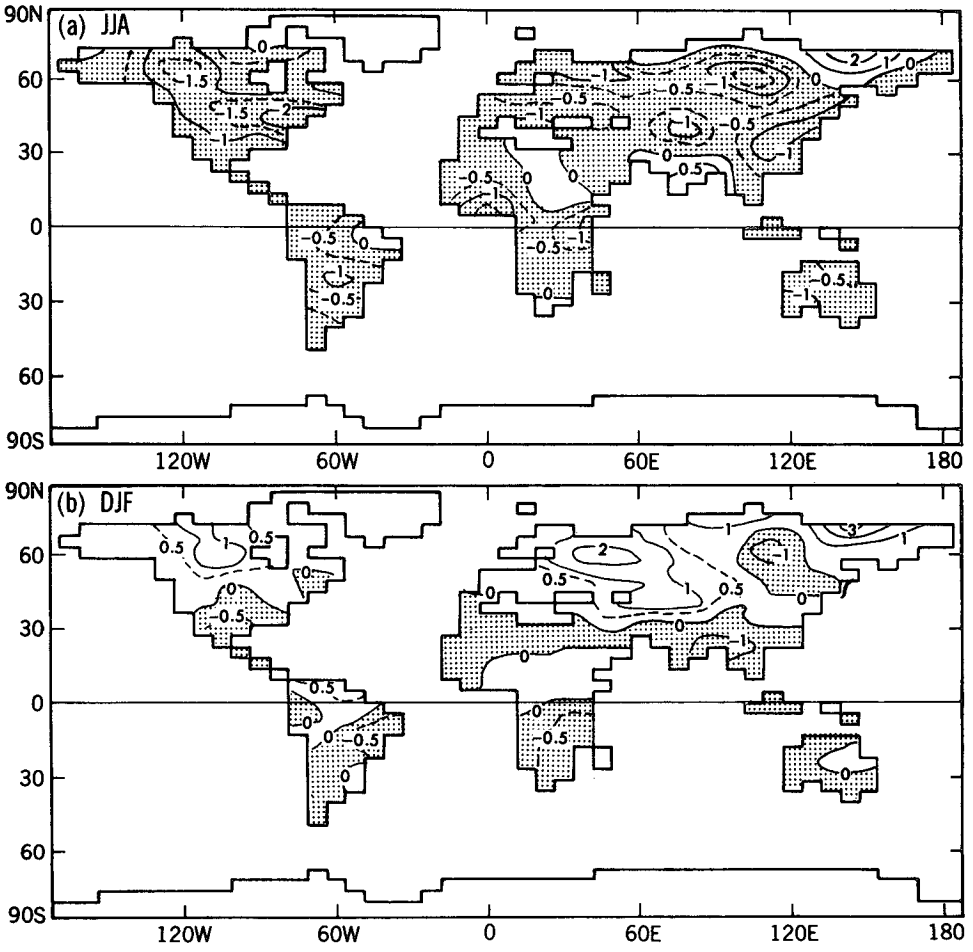

FIG. 20. The geographical distributions of the difference in soil moisture (cm) between the G (60th–80th year) and S (0–100th year) integrations. (a) June–August. (b) December–February.

tively large over Australia and the subtropical region of South America, resulting in the winter reduction of zonal-mean soil moisture around 30°S latitude in Fig. 12b.

In the December–February period, soil moisture increases over most of the middle and high latitudes of the Northern Hemisphere, though it is reduced slightly over the regions in eastern Canada and eastern Siberia. The increase is relatively large over the central portion of Canada and the extensive region in the western portion of the Russian Republic that stretches from Scandinavia to the western portion of the Russian Republic. On the other hand, soil moisture is reduced in the Northern Hemisphere subtropics. The reduction is relatively large over Mexico and Southeast Asia (i.e., Indochina and India), resulting in the reduction of zonal-mean soil moisture around 25° latitude as indicated in Fig. 12b.

The change of June–August soil moisture discussed above may be compared with the interannual variability (i.e., standard deviation) of seasonal mean soil moisture shown in Fig. 21 [see the studies of Delworth and Manabe (1988, 1989) for extensive discussions of soil moisture variability]. The ratio between these two quantities represents the so-called signal-to-noise ratio (e.g., Wigley and Jones 1981) of the change. According to this comparison, the change of soil moisture is comparable to the interannual variability of seasonal mean soil moisture in middle and high latitudes of the Northern Hemisphere. However, in low latitudes and in the Southern Hemisphere where the change is relatively small, it tends to be less than the standard deviation of seasonal mean soil moisture. Thus, the signal of the change is likely to be obscurred by the noise of natural variability in these regions. This is consistent with the results of Manabe and Wetherald (1985, 1987) in which the pattern of soil moisture change often varied from one equilibrium experiment to another in the Southern Hemisphere and tropical portions of continents.

To examine the evolution of the change of soil moisture in the CO_2 growth experiment, the geographical distributions of the change of June–August soil moisture in both the North American and Eurasian continents are averaged over three 20-year intervals of the 40th–60th, 60th–80th, and 80th–100th years and are illustrated in Figs. 22 and 23. For comparison, the corresponding change of soil moisture obtained from the CO_2 reduction experiment is also illustrated.

Figure 22 indicates that, in the CO_2 growth experiment, a region of relatively large soil moisture reduction over the North American continent appears in and near the northeastern part of the United States in the 40th–60th-year interval, but establishes itself over a wide belt stretching from the East Coast to the western portion of Canada during the 60th–80th- and 80th–100th-year intervals. Over the Eurasian continent (Fig. 23) a region of relatively large soil moisture reduction becomes evident by the 60th–80th year in the nearly zonal belt around 60°N and the localized regions situated around 45°N (i.e., extreme western and eastern China, and southern Europe) and becomes well established by the 80th–100th-year interval. In summary, a nearly self-similar pattern of the CO_2-induced soil moisture change is maintained in the Northern Hemisphere during the 60th–80th-year and the 80th–100th-year intervals of the CO_2 growth experiment.

In the CO_2 reduction experiment, the change of June–August soil moisture tends to have opposite sign but a similar broad-scale pattern with the change obtained from the CO_2 growth experiment. The approximate antisymmetry between the two responses to the opposite forcings suggests that an essentially similar mechanism controls both soil moisture responses, underscoring the consistency between the results from the two experiments.

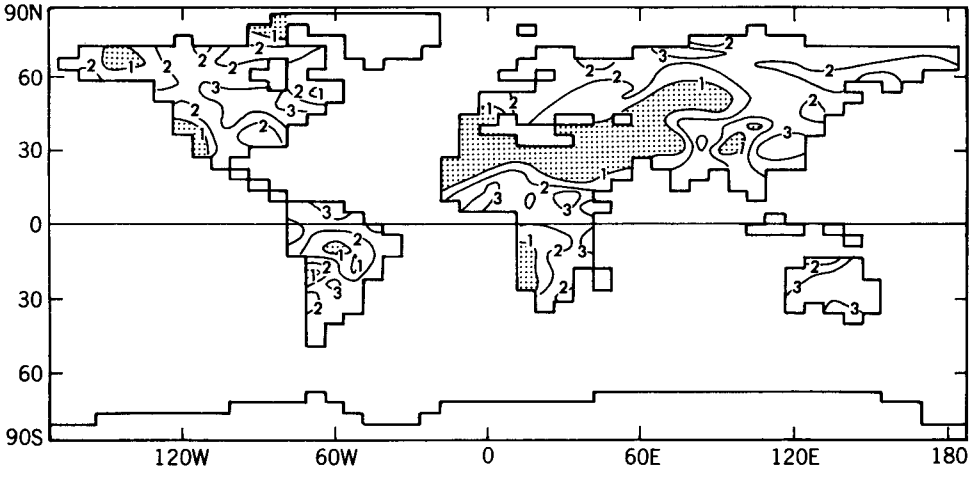

FIG. 21. Geographical distribution of the standard deviation of seasonal mean soil moisture (June–August) computed using 100 years of the S integration. Units are in centimeters.

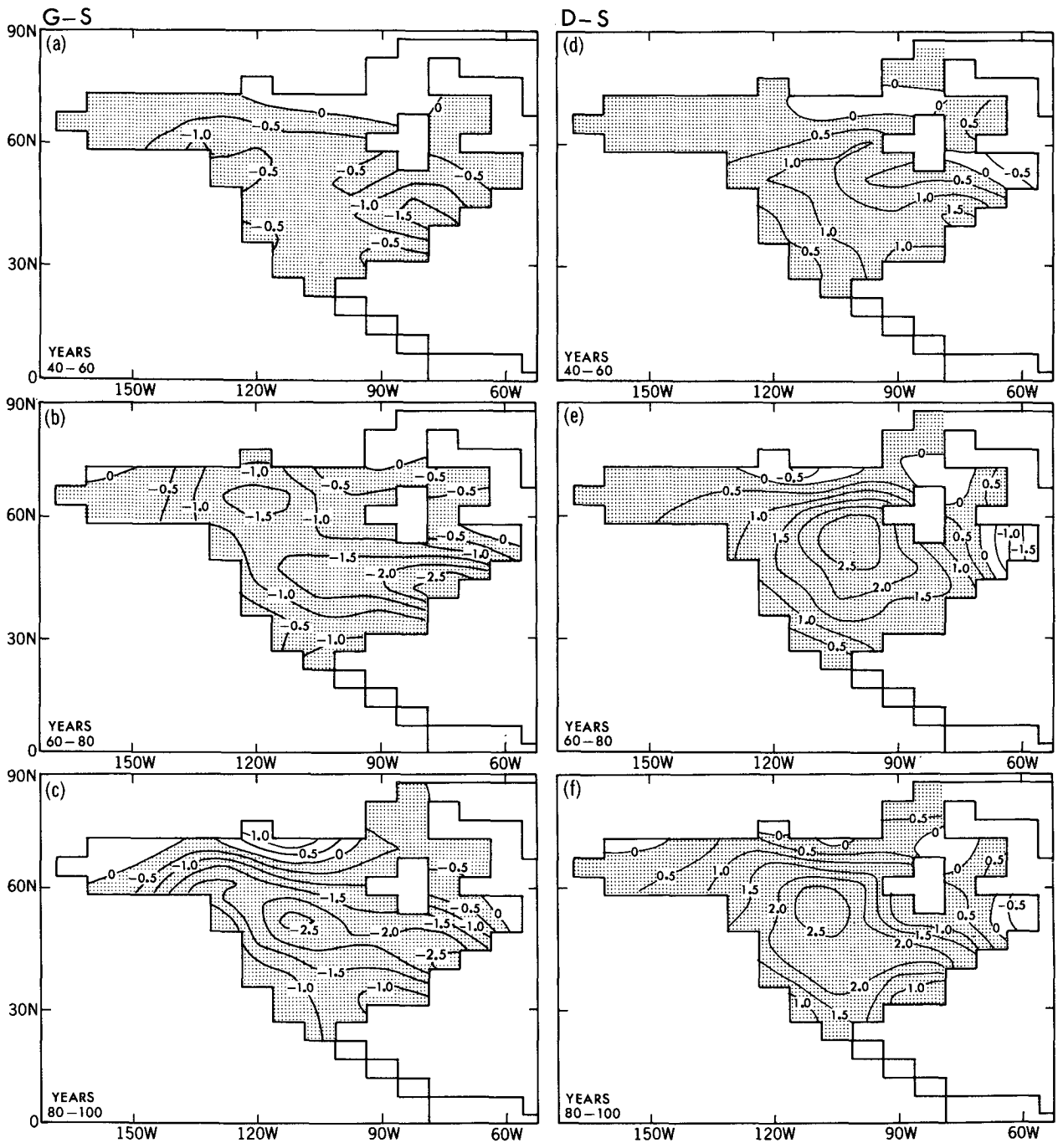

FIG. 22. The geographical distribution of the difference in June–August soil moisture (cm) over the North American continent between the G integration averaged over (a) 40th–60th year, (b) 60th–80th year, (c) 80th–100th year and the S integration. The distribution of corresponding soil moisture difference between the D integration averaged over (d) 40th–60th year, (e) 60th–80th year, (f) 80th–100th year and the S integration. The soil moisture from the S integration was averaged over the entire 100-year period.

6. Summary and conclusions

This study investigates the seasonal dependence of the climate response of a coupled ocean–atmosphere model to gradual changes of atmospheric carbon dioxide. By comparing the transient response of the coupled model at the time of the doubling (or halving) of atmospheric carbon dioxide with the equilibrium response of the atmosphere mixed-layer ocean model to the CO_2 doubling (or halving), the influence of the thermal inertia of the oceans upon the transient response was investigated.

It was found that, in response to a gradual increase of atmospheric carbon dioxide, the increase of surface air temperature is at a maximum over the Arctic Ocean

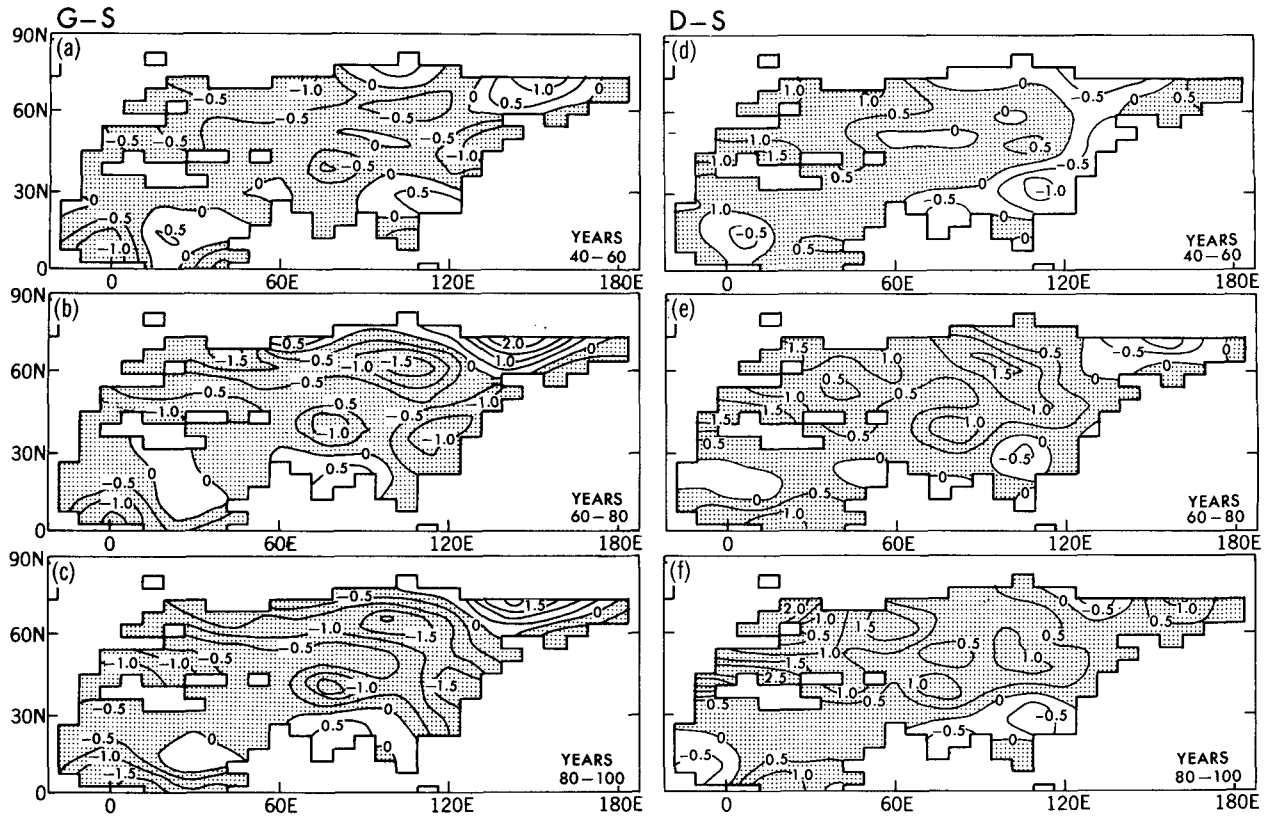

FIG. 23. Same as Fig. 22 except for the Eurasian continent.

and its surroundings in the late fall and winter. On the other hand, the Arctic warming is at a minimum in summer. The mechanism responsible for the seasonal dependence of the surface air temperature change described above is essentially similar to the results from an equilibrium experiment conducted earlier (Manabe and Stouffer 1979, 1980) with an atmosphere–mixed-layer ocean model. Because of the existence of a halocline with very stable stratification, the heat exchange between the mixed layer and deeper ocean is very small in the Arctic Ocean of the coupled ocean–atmosphere model used here. Therefore, it is not surprising that the seasonal dependence of surface air temperature change in the coupled model is qualitatively similar to the response of an atmosphere–mixed-layer ocean model in which the heat flux at the bottom of the mixed layer is unchanged.

In sharp contrast to the situation in the Arctic Ocean, the increase of surface air temperature and its seasonal variation in the circumpolar ocean of the Southern Hemisphere are very small due to the deep vertical mixing of water, as discussed in Part I of this study. Thus, the maximum warming during the cold season does not materialize in the circumpolar ocean. This is quite different from the results of the present and earlier equilibrium experiments, which indicate the maximum warming during the cold season.

The gradual increase of atmospheric carbon dioxide affects not only the seasonal variation of the lower tropospheric temperature but also that of land surface hydrology. For example, in response to the CO_2 increase, soil moisture is reduced during the June–August period over most of the continental regions, with the notable exception of the Indian subcontinent, where precipitation and soil moisture increase. The summer reduction of soil moisture in the Northern Hemisphere is relatively large over the regions stretching from the northern United States to western Canada, eastern China, southern Europe, Scandinavia, and most of the Russian Republic, in qualitative agreement with results from equilibrium experiments conducted in the present and some earlier studies by use of an atmosphere–mixed-layer ocean model.

During the December–February period, soil moisture increases in middle and high latitudes of the Northern Hemisphere. For example, the increase is relatively large over the western part of the Russian Republic and the central portion of Canada. On the other hand, it is reduced in the subtropics particularly over Southeast Asia and Mexico. The reduction of soil moisture is also notable in the subtropical portion of the continents in the Southern Hemisphere in winter (i.e., June–August period), although the regions of relatively large reduction change with time as influenced by the natural variability of the model climate.

The broad features of soil moisture change and its

seasonal variation in the present experiment are qualitatively similar to the change in the equilibrium experiments conducted in the present and many earlier studies. According to the analysis of the water budget at the continental surface, the mechanisms involved in these changes are also similar between the transient and equilibrium experiments. One can detect, however, another mechanism that reduces soil moisture and runoff over the continents in middle and high latitudes of the Northern Hemisphere in the transient experiment. Because of the thermal inertia of the ocean, the increase of sea surface temperature is reduced substantially in middle and high latitudes as compared with the equilibrium response experiment. Thus, the increase in oceanic evaporation and, accordingly, that of moisture transport from the oceans to continents are not as large as they would be without the delay in the warming of the sea surface, resulting in the reduction of precipitation, soil moisture, and runoff over the continents poleward of 30° latitude in the Northern Hemisphere.

The transient response of surface temperature and soil moisture described above is opposite in sign but has seasonal and geographical distributions that broadly resemble the response to the gradual reduction of atmospheric carbon dioxide. This antisymmetry of response between the CO_2 growth and CO_2 reduction experiments underscores that these changes are CO_2 induced and are controlled by similar mechanisms. On the other hand, many small-scale features not shared by these two experiments may be indicative of natural climate variation and may not be CO_2 induced.

The results from many equilibrium experiments reveal that the change of climate critically depends upon the climate simulated by the control integration. For example, the summer reduction of soil moisture in an equilibrium CO_2 doubling experiment fails to materialize in those regions where soil moisture is very small in the control integration. In view of the fact that the simulation of climate by the present model is far from satisfactory, one should not take too literally the geographical details of the changes of climate obtained here. A more realistic simulation of precipitation is required for a reliable estimate of soil moisture change.

In assessing the results from the present study, it is important also to note that the parameterization of the land surface process was subjected to the maximum simplification and the computational resolution of the models used here is far from sufficient. Furthermore, the fluxes of heat and water at the ocean–atmosphere interface were adjusted to prevent drift at the coupled model toward an unrealistic state. (See also Sausen et al. 1988; Manabe and Stouffer 1988.) It is therefore desirable to repeat the present study by use of a model with higher computational resolution and improved parameterization of land surface processes.

Acknowledgments. The authors are very grateful to I. M. Held, J. D. Mahlman, P. C. D. Milly, J. F. B. Mitchell, D. Rind, and R. T. Wetherald, who reviewed early versions of the manuscript and gave many valuable comments. In particular, J. F. B. Mitchell gave much advice which, in our opinion, significantly enhanced the readability of the paper. It is a great pleasure to thank K. Bryan and K. Dixon, whose advice and assistance were indispensable for the completion of this study. J. Kennedy and P. Tunison helped in the preparation of the manuscript and figures. J. D. Mahlman, Director of the Geophysical Fluid Dynamics Laboratory of NOAA, gave wholehearted support throughout the course of this study.

REFERENCES

Bryan, K., F. G. Komro, S. Manabe, and M. J. Spelman, 1982: Transient climate response to increasing atmospheric carbon dioxide. *Science,* **215,** 56–58.

——, S. Manabe, and M. J. Spelman, 1988: Interhemispheric asymmetry in the transient response of a coupled ocean–atmosphere model to a CO_2 forcing. *J. Phys. Oceanogr.,* **18,** 851–867.

Crutcher, H. L., and M. Meserve, 1970: Selected level heights, temperatures and dew points for the Northern Hemisphere. NAVAIR 50-1C-52, U.S. Naval Weather Service, Washington, D.C., 17 pp. plus 144 charts.

Delworth, T., and S. Manabe, 1988: The influence of potential evaporation on the distribution of soil moisture and climate. *J. Climate,* **1,** 523–547.

——, and ——, 1989: The influence of soil wetness on atmospheric variability. *J. Climate,* **2,** 1447–1462.

Hansen, J., A. Lacis, D. Rind, G. Russell, P. Stone, I. Fung, R. Ruedy, and J. Lerner, 1984: Climate sensitivity: Analysis of feedback mechanisms. Climate Processes and Climate Sensitivity, *Geophys. Monogr.,* **29,** Maurice Ewing Vol. 5, J. E. Hansen and T. Takahashi, Eds., AGU, 130–163.

——, I. Fung, A. Lacis, D. Rind, S. Lebedeff, R. Ruedy, G. Russell, and P. Stone, 1988: Global climate changes as forecast by the Goddard Institute for Space Studies three dimensional model. *J. Geophys. Res.,* **93,** 9341–9364.

Held, I. M., 1982: Climate models and the astronomical theory of the ice ages. *Icarus,* **50,** 449–461.

Jaeger, L., 1976: Monthly precipitation maps for the entire earth (in German). *Ber. Deutsch Wetterdienstes,* **18**(139), 38 pp.

Kellog, W. W., and Z-C. Zhao, 1988: Sensitivity of soil moisture to doubling of carbon dioxide in climate model experiments. Part I: North America. *J. Climate,* **1,** 348–366.

Manabe, S., and R. J. Stouffer, 1979: A CO_2-climate sensitivity study with a mathematical model of the global climate. *Nature,* **282,** 491–493.

——, and ——, 1980: Sensitivity of a climate model to an increase of CO_2 concentration in the atmosphere. *J. Geophys. Res.,* **85**(C10), 5529–5554.

——, and R. T. Wetherald, 1985: CO_2 and hydrology in "Issues in Atmospheric and Oceanic modeling." *Advances in Geophysics,* Vol. 28A, Academic Press, 131–157.

——, and ——, 1987: Large scale changes of soil wetness induced by an increase in atmospheric carbon dioxide. *J. Atmos. Sci.,* **44,** 1211–1235.

——, ——, and R. J. Stouffer, 1981: Summer dryness due to an increase of atmospheric CO_2 concentration. *Clim. Change,* **3,** 347–386.

——, K. Bryan, and M. J. Spelman, 1990: Transient response of a global ocean–atmosphere model to a doubling of atmospheric carbon dioxide. *J. Phys. Oceanogr.,* **20,** 722–749.

——, R. J. Stouffer, M. J. Spelman, and K. Bryan, 1991: Transient response of a coupled ocean–atmosphere model to gradual changes of atmospheric CO_2. Part I: Annual mean response. *J. Climate,* **4,** 785–818.

Meehl, G. A., and W. M. Washington, 1988: A comparison of soil

moisture sensitivity in two global climate models. *J. Atmos. Sci.*, **45**, 1476–1492.

Mitchell, J. F. B., and D. A. Warrilow, 1987: Summer dryness in northern mid-latitudes due to increased CO_2. *Nature*, **330**, 238–240.

——, C. A. Wilson, and W. M. Cunnington, 1987: On CO_2 climate sensitivity and model dependence of results. *Quart. J. Roy. Meteor. Soc.*, **113**, 293–322.

——, S. Manabe, V. Meleshko, and T. Tokioka, 1990: Equilibrium climate change and its implications for the future. Climate Change: IPCC Scientific Assessment, J. T. Houghton, G. J. Jenkins and J. J. Ephraums, Eds. Cambridge University Press, 131–164.

Rind, D., R. Goldberg, J. Hansen, C. Rosenzweig, and R. Ruedy, 1990: Potential evapotranspiration and the likelihood of future drought. *J. Geophys. Res.*, **95**(D7), 9983–10 004.

Sausen, R., K. Barthel, and K. Hasselmann, 1988: Coupled ocean–atmosphere models with flux correction. *Climate Dyn.*, **2**, 145–163.

Schlesinger, M. E., and J. F. B. Mitchell, 1987: Climate model simulations of the equilibrium climatic response to increased carbon dioxide. *Rev. Geophys.*, **25**, 760–798.

Spelman, M. J., and S. Manabe, 1984: Influence of oceanic heat transport upon the sensitivity of a model climate. *J. Geophys. Res.*, **89**, 571–586.

Taljaard, J. J., H. van Loon, H. L. Crutcher, and R. L. Jenne, 1969: Climate of the upper air. Part I: Southern Hemisphere, NAVAIR 50-1C-55, U.S. Naval Weather Service, Washington, D.C., 135 pp.

Washington, W. M., and G. A. Meehl, 1984: Seasonal cycle experiment on the climate sensitivity due to a doubling of CO_2 with an atmospheric general circulation model coupled to a simple mixed layer ocean model. *J. Geophys. Res.*, **89**, 9475–9503.

——, and ——, 1989: Climate sensitivity due to increased CO_2: Experiments with a coupled atmosphere and ocean general circulation model. *Climate Dyn.*, **4**, 1–38.

Wigley, T. M. L., and P. D. Jones, 1981: Detection of CO_2-induced climate change. *Nature*, **292**, 205–208.

Wilson, C. A., and J. F. B. Mitchell, 1987: A doubled CO_2 climate sensitivity experiment with a global climate model including a simple ocean. *J. Geophys. Res.*, **92**(D11), 13 315–13 343.

Zhao, Z-C., and W. W. Kellog, 1988: Sensitivity of soil moisture to doubling of carbon dioxide in climate model experiments. Part II: The Asian monsoon region. *J. Climate*, **1**, 367–378.